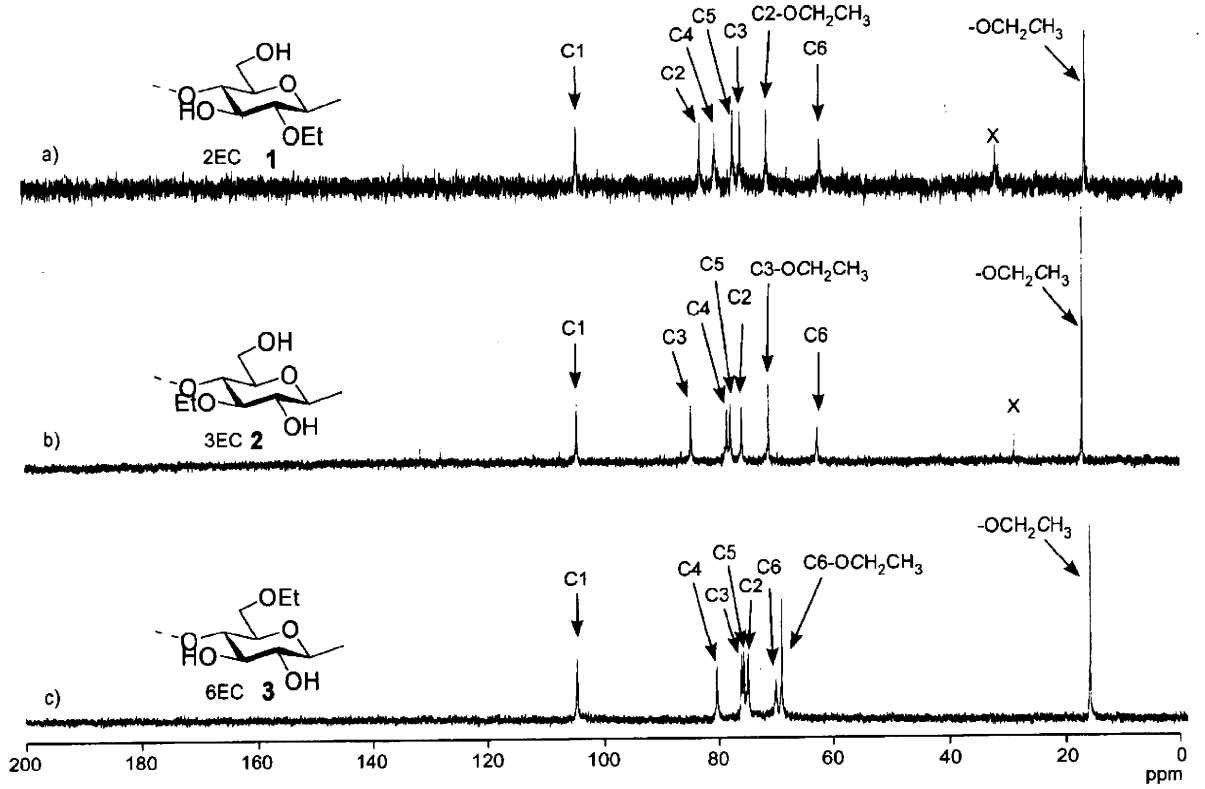

■ *Figure 3.* ^{13}C NMR spectra of compound **1**, **2** and **3**, measured in D_2O.

molecular weights of polymerization products **7**, **11**, **12-1**, **12-2** and **12-3** were different to each other. Cellulose derivatives with different DPs could be obtained according to the polymerization conditions. However, 2EC (1) with a higher DP could not be obtained because 2EC was polymerized via the ring-opening polymerization of 3,6-di-*O*-benzyl-α-D-glucopyranose 1,2,4-orthopivalate and 3,6-di-*O*-benzyl-2-*O*-pivaloyl-(1 → 4)-β-D-glucopyranan with maximum DP ca. 20, and was synthesized after many trials.[15] One and three polymerization conditions were carried out for 3EC (**2**) and 6EC (**3**), respectively. Run 4 has been reported in our previous paper.[8]

The final products, 2EC (**1**), 3EC (**2**) and 6EC (**3**), were water soluble. Their ^1H and ^{13}C NMR spectra measured in D_2O are shown in Figure 2 and Figure 3, respectively. The H1 of compound **1** appeared at 4.53 ppm as a doublet with $J = 7.5$ Hz, indicating the β-linkage. The H2 of compound **1** appeared at 3.18 ppm. Other ring protons appeared in the range from 3.3 to 4.2 ppm. Furthermore, ring proton signals of compound **2** were assigned as shown in Figure 2(b). The H1 of compound **2** appeared at 4.50 ppm as a doublet with $J = 6.9$ Hz indicating the β-linkage. The H2 of compound **2** appeared at 3.32 ppm. On the other hand, ring proton signals of compound **3** were overlapping, except for H1 and H2. The H1 of compound **3** appeared at 4.43 ppm as a doublet with $J = 7.8$ Hz indicating the β-linkage. The H2 of compound **2** appeared at 3.20 ppm. The ^{13}C NMR chemical shifts of compounds **1**, **2**, and **3** are summarized in Table 2. All carbons were assigned by means of two-dimensional NMR measurements. Carbons where the hydroxyl group is

■ *Table 2.* ^{13}C chemical shifts of compounds **1**, **2** and **3** in D_2O (DSS as external standard).

Compound	R2	R3	R6	C1	C2	C3	C4	C5	C6	CH_2CH_3	CH_2 CH_3
1	Et	H	H	104.9	83.5	76.3	80.8	77.7	62.5	71.8	17.2
2	H	Et	H	104.8	76.0	84.9	78.7	77.9	62.8	71.2	17.3
3	H	H	Et	105.1	75.5	76.6	80.9	76.1	70.7	69.6	16.8

Table 3. Solubilities of *O*-ethyl-celluloses **1**, **2** and **3**. Solubility was evaluated at a concentration of 5 wt.-%. ++: Clear solution; +: colloidal dispersion; -: precipitation.

Solvent	δ	Compound No.		
		1	**2**	**3-1, 3-2**
H_2O	21.0	+	+	+
H_2O[a)]	21.0	+	++	++
MeOH	12.9	+	++	+
EtOH	11.2	-	-	-
Acetone	9.4	-	-	-
$CHCl_3$	9.1	-	-	-
THF	9.1	-	-	-
$MeOH/CH_2Cl_2$ (1:4, v/v)	-	+	-	++
$EtOH/H_2O$ (1:1, v/v)	-	+	++	+

[a)]Concentration: 1 wt.-%.

ethylated appeared at approx. 7–8 ppm lower magnetic field, compared to carbons where hydroxyl groups existed. The synthesis of tri-*O*-ethyl-cellulose has already been reported by Isogai et al.[17]. Our NMR data agree with data in this report. In the carbon NMR spectrum of compound **2**, the peak appearing at 32.5 ppm is that of an impurity. It was confirmed in the NMR spectra of 3,6-di-*O*-benzyl-2-*O*-ethyl-cellulose (**9**) that the pivaloyl group was completely removed and the ethyl group was introduced at the C2 position (the NMR spectrum is not shown).

There is no remarkable difference in the water solubilities among the three regioselective mono-*O*-ethyl celluloses, as shown in Table 3. Compound **1**, having an ethyl group at the C2 position tended to make a colloidal dispersion in some solvents, such as water and mixed solvent systems. In summary, it was found that all mono-*O*-ethylated celluloses **1**, **2**, and **3** were hydrophilic.

X-ray Analysis

The 2-*O*-ethyl cellulose **1** in the solid phase was amorphous, judged from its X-ray diffractogram, which is shown in Figure 4(a). In the case of the 3-*O*-ethyl cellulose **2**, a peak appeared at 2θ = approx. 10° with the amorphous background. In the case of the 6-*O*-ethyl cellulose **3-2**, two peaks appeared at 2θ = approx. 6° and 21.5° with the amorphous background. As mentioned above, the amorphous 2-*O*-ethyl cellulose **1** has poor solubility, compared with compound **2** and **3**. Thus, there was no relationship between the crystallinities of mono-*O*-ECs **1**, **2** and **3** and their solubilities in water and other solvents.

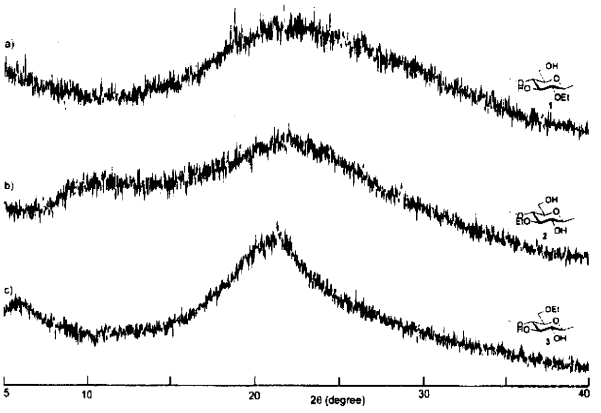

Figure 4. X-ray diffractograms of compounds **1**, **2** and **3-2**.

Surface Activities of 2-*O*-, 3-*O*- and 6-*O*-Ethylcelluloses

The surface tension of aqueous solutions of mono-ethylated celluloses was measured by the Wilhelmy plate method. The experimental data indicated that compounds **1**, **2**, and **3** were completely or partly soluble in water. However, there was no obvious difference in the surface activities in water among compounds **1**, **2** and **3-3**, as shown in Figure 5. The surface tension of compounds **1**, **2** and **3-3** at 0.5 wt.-% in distilled water was in the range 36–39 $mN \cdot m^{-1}$ at 20 °C, and surface activities of compounds **1**, **2** and **3-3** over 0.1 wt.-% (1 $mg \cdot mL^{-1}$) were better than that of commercial methylcellulose SM-4.

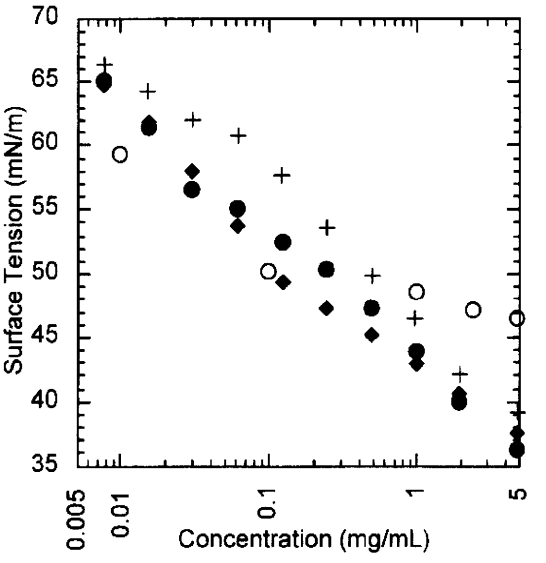

Figure 5. Surface tension measurements of compounds **1**, **2** and **3-2**. +: 2EC (**1**); solid diamond: 3EC (**2**); solid circle: 6EC (**3-2**); open circle: methylcellulose SM-4.

Macromol. Biosci. **2010**, *10*, 638–647

DOI: 10.1002/mabi.200900392

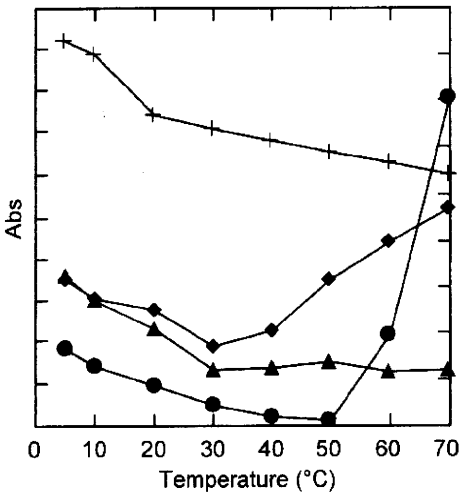

Figure 6. Temperature-dependent turbidity tests of compounds **1**, **2**, **3-1** and **3-2**. +: compound **1**; solid diamond: compound **2**; solid triangle: compound **3-1**; solid circle: compound **3-2**.

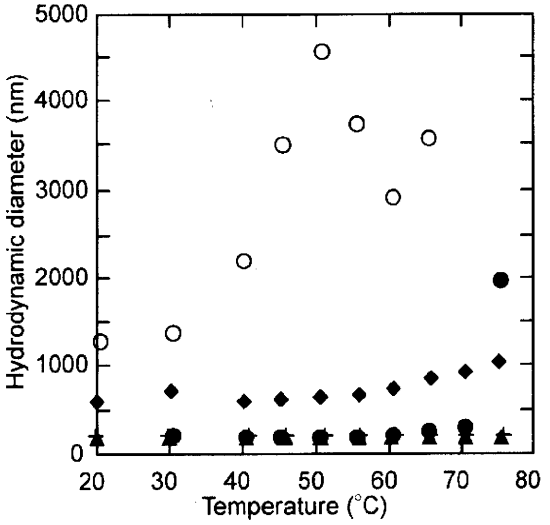

Figure 7. Dynamic light scattering experiments of compounds **1**, **2**, **3-1**, **3-2**and **3-3**. +: compound **1**; solid diamond: compound **2**; solid triangle: compound **3-1**; solid circle: compound **3-2**; open circle: compound **3-3**.

Thermal Properties of 2-*O*-, 3-*O*- and 6-*O*-Ethylcelluloses

Turbidities of 2-*O*-, 3-*O*- and 6-*O*-Ethylcelluloses

Temperature dependent turbidity tests of aqueous solutions of compounds **1**, **2**, and **3** (1.0 wt.-%) were carried out by means of UV-vis spectroscopy at a wavelength of 660 nm. The 2EC (**1**) did not show a thermo-responsive property, as shown in Figure 6. The 3EC (**2**), however, started clouding at approximately 40 °C. It was only a clouding point. Namely, an aqueous solution of compound **2** did not become gel state, although Koschella et al. reported that 3EC (**2**) shows thermo-reversible gelation.[14] On the other hand, 6EC (**3-2**) showed a cloud point at approx. 60 °C, whereas 6EC (**3-1**) with a lower molecular weight did not. These clouding temperatures were lower than those detected by dynamic light scattering experiments and DSC measurements, as described later. The turbidity test might be sensitive for the starting temperature to detect a turbid solution. Interestingly, the aqueous solution of compound **3-3** showed thermo-reversible gelation behavior at approx 70 °C, as described later. Compounds **1**, **2**, **3-1**, **3-2** and **3-3** were acetylated and their molecular weight was calculated again by means of GPC in order to confirm their molecular weight again, as shown in Table 4. It was confirmed that these compounds did not decompose under deprotection and substitution processes.

Dynamic Light Scattering Experiments and Visual Observation of EC Solutions in Water

Aggregation behaviors of compounds **1**, **2** and **3** were investigated depending on the temperature between 10 and 75 °C. The hydrodynamic diameter of a 1% aqueous solution of compound **1** (2EC) did not change in the whole range of tested temperatures, as shown in Figure 7. The hydrodynamic diameter of compound **2** (3EC) increased gradually with increasing the temperature from ca. 40 °C. This fact agrees with the previous work of Koschella et al.[14] The hydrodynamic diameter of compound **3-2** (6EC, DP 60.3) increased suddenly at 70–75 °C. On the other hand, the hydrodynamic diameter of compound **3-3** (6EC. DP 36.1) was over 1 000 nm and larger than those of other

Table 4. Molecular weights and DPs of acetylated ethylcelluloses.

Compound	R_2	R_3	R_6	$\overline{M}_w$ (10^3)	$\overline{M}_n$ (10^3)	$\overline{M}_w/\overline{M}_n$	DP_w	DP_n
Acetylated **1**	Et	Ac	Ac	3.9	2.9	1.32	14.0	10.6
Acetylated **2**	Ac	Et	Ac	22.8	13.6	1.68	83.2	49.4
Acetylated **3-1**	Ac	Ac	Et	6.3	3.5	1.77	22.8	12.9
Acetylated **3-2**	Ac	Ac	Et	29.3	16.6	1.77	107.0	60.3
Acetylated **3-3**	Ac	Ac	Et	15.0	9.9	1.51	54.6	36.1

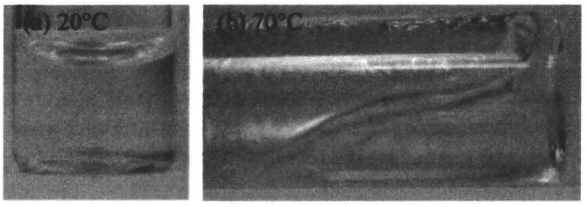

Figure 8. Visual observation of aqueous solution of compound **3-3** (1 wt.-%) a) 20 °C; b) 70 °C.

compounds **1**, **2**, **3-1** and **3-3**, and increased in proportion to temperature. Only compound **3-3** showed such a peculiar aggregation property in water. Moreover, the aqueous solution of compound **3-3** became a gel, as shown in Figure 8. Namely, 6EC (**3-3**, DP 36.1) showed a thermo-reversible gelation behavior. An appropriate molecular weight of ethyl cellulose derivative for gelation behavior might exist. However, the reason could not be elucidated up to now. Further investigation on this aggregation process is needed.

DSC Measurements of Compounds 1, 2 and 3

The thermal properties of compound **1**, **2** and **3-2** were studied by means of DSC measurements. The heating and cooling curves are shown in Figure 9 and 10, respectively. The DSC data for **3-2** has been reported in our previous paper.[8] There was no obvious character in either the heating and cooling curves of the 2EC (**1**). This fact agreed with the data from its turbidity test and DLS experiments. The ethyl group at the C2 position may be hard to hydrate at ambient temperature, whereas compound **1** has a lower molecular weight, such as DP 11. The 2EC (**1**), having ethyl groups at the C2 position along the cellulose chains, possesses different thermal character compared to the ethyl groups at the C3 or C6 positions, judging from our experimental data.

Koschella et al. reported a temperature-induced change of turbidity of 3-*O*-ethyl-cellulose in water.[14] The aqueous

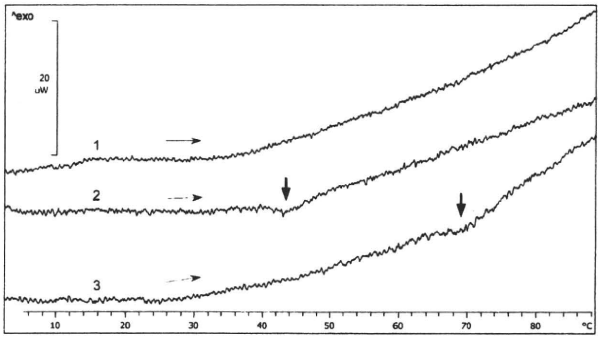

Figure 9. DSC heating curves of aqueous solutions of compounds **1**, **2** and **3-2** (concentration = 1.0 mg/10 μL of water). Heating rate: 0.5 K · min^{-1}.

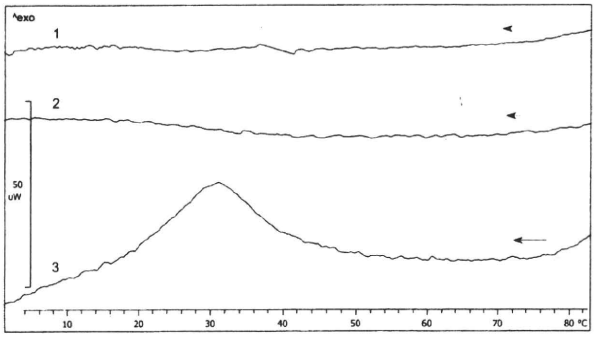

Figure 10. DSC cooling curves of aqueous solutions of compounds **1**, **2** and **3-2**. Cooling rate: 3.0 K · min^{-1}.

solution of the 3-*O*-ethyl-cellulose from natural cellulose shows thermo-reversible gelation when heated up to 58.5 °C. On the other hand, the aqueous solution of our 3EC (**2**) via a synthetic cellulose derivative did not show thermo-responsive gelation. However, a clear aqueous solution of 3EC (**2**) turned opaque at around 80 °C, indicating that compound **2** is a polymer having a LCST. In the heating curve of compound **2**, an endothermic peak was detected at about 40 °C, as shown in Figure 9. This fact agreed with the data from the turbidity test, as shown in Figure 6, namely, dehydration occurred during the heating process. However, the cooling curve of 3EC (**2**) showed no obvious peak (Figure 10).

In the case of 6-*O*-ethyl-celluloses (**3-2**), endothermic and exothermic peaks were observed in the heating and cooling curves, respectively. 6EC (**3-2**) possessed a LCST at about 70 °C, becoming a turbid solution. Thus, the results of DSC measurements of 6EC (**3-2**) agreed with those of the turbidity test and the visual observation of the solution. Consequently, 6EC (**3-2**) showed thermo-responsive properties. On the other hand, there was no peak found for the DSC curves of 6ECs (**3-1** and **3-3**). Namely, endo- and exo-thermic peaks of the compound **3-3** could not be observed, whereas compound **3-3** showed a thermo-reversible gelation at approx. 70 °C. The DP-dependent thermal behavior of regioselectively-ethylated celluloses is now under investigation using cellulose derivatives with different DPs.

Conclusion

Among three regioselectively ethylated cellulose derivatives **1**, **2** and **3** synthesized by ring-opening polymerizations of glucopyranose 1,2,4-orthopivalate derivatives **4**, **5** and **6**, respectively, the 3-*O*- (**2**) and 6-*O*- (**3**) ethyl-celluloses over DP_n 36 were thermo-responsive in water. The 2-*O*-ethyl-cellulose (**1**) having a $DP_n = 11$ did not show such a property. The 2-*O*-ethyl-cellulose with a higher DP, however, might have thermo-responsive properties. Further-

Macromol. Biosci. **2010**, *10*, 638–647

Macromolecular Journals

DOI: 10.1002/mabi.200900392

more, a factor of molecular weight was found to be of importance for the thermal properties of 6-*O*-ethylcellulose (**3**) in water. Only the aqueous solution of compound **3-3** having DP = 36 showed thermo-reversible gelation behavior at 70–75 °C on heating. In addition, compounds **2** and **3-2** showed a LCST at about 40 °C and 70 °C, respectively. The thermo-responsive temperature could be controlled by the position of the ethyl group on the cellulose molecules, whereas water soluble ethyl cellulose has been reported to show gelation behavior at 30 °C.[2]

Experimental Part

Measurements

The ^{1}H and ^{13}C NMR spectra were recorded on a Varian INOVA 300 spectrometer in chloroform-*d* with tetramethylsilane as an internal standard, by using pulse sequences for one- and two-dimensional spectra. Gel permeation chromatography (GPC) measurements were carried out at 40 °C using a GPC system (CBM-20A, SIL-10A, LC-10ATvp, CTO-10Avp, SPD-10Avp and RID-10A, Shimadzu, Japan). Shodex columns (K802, K802.5 and K805) were used. Number and weight averaged molecular weights ($\overline{M}_n$, $\overline{M}_w$) and polydispersity index ($\overline{M}_w/\overline{M}_n$) were estimated using polystyrene standards (Shodex). Chloroform was used as an eluent. The flow rate was 1.0 mL · min^{-1}. X-ray diffractograms were recorded on a RINT2200V (RIGAKU, Co. Ltd. Japan). The surface tensions of aqueous solutions of compounds **1**, **2** and **3** was measured at room temperature (ca. 20 °C) on a CBVP-A3 (Kyowa Interface Science Co, Ltd., Japan) by the Wilhelmy plate method, as reported previously.[10] A Teflon cell with 700 μL of solution was used for the measurements. Surface tension gradually decreased during the measurements. The values were used when the values were stable after 20 to 120 min. Turbidity tests of aqueous solutions of compounds **1**, **2** and **3** were measured on a Jasco V-560 UV-vis spectrometer equipped with a temperature controller EHC-477T. The wavelength of the measurements was 660 nm. The band width was 2.0 nm. Dynamic light scattering data were recorded on a particle size analyzer ELSZ-2 (Otsuka Electronics, Japan). The hydrodynamic diameter was obtained using the cumulant method. The differential scanning calorimetry (DSC) curves of aqueous solutions of compounds **1**, **2** and **3** were obtained on a Mettler-Toledo DSC823e with an HSS7 sensor. The aqueous solutions were sealed in aluminum pans. The samples were cooled to 0 °C, kept at that temperature for 120 min, and then heated up to 90 °C (heating rate: 0.5 K · min^{-1}). After keeping the temperature at 90 °C for 10 min, the samples were cooled to 0 °C (cooling rate: 3.0 K · min^{-1}). This cycle was repeated 4 times.

Polymerization

All polymerizations were carried out as described in previous papers.[15,16] Boron trifluoride diethyl etherate was used as an initiator of the cationic ring-opening polymerization of glucose orthopivalate derivatives. Polymerizations were terminated by adding cold methanol at the polymerization temperature. After dilution with ethyl acetate, the polymer solution was washed with water. The solution was dried over anhydrous sodium sulfate and concentrated to dryness. Generally, when the remaining monomers were found by TLC analyses after the ring-opening polymerization, *n*-hexane was added to the polymer mixture to remove the remaining monomer while applying ultrasonic waves. The residual polymer was finally dried in vacuo.

Synthesis Route for 2-*O*-Ethyl Cellulose (1)

3,6-Di-*O*-benzyl-2-*O*-pivaloyl Cellulose (7)

Compound 7 was obtained according to our method in the literature.[15] Polymerization of 3,6-di-*O*-benzyl-2-*O*-pivaloyl-α-D-glucopyranose 1,2,4-orthopivalate (**4**) (150 mg, 0.552×10^{-3} mol) was carried out for 12.3 h at −10 °C. 3,6-Di-*O*-benzyl-2-*O*-pivaloyl cellulose (**7**) (139.9 mg, 93% yield) was obtained. No monomer remained after polymerization ($DP_n = 17.8$, $\overline{M}_n = 7.60 \times 10^3$, $\overline{M}_w/\overline{M}_n = 1.56$).

3,6-Di-*O*-benzyl Cellulose (8)

To a solution of 3,6-di-*O*-benzyl-2-*O*-pivaloyl cellulose (**7**) (125.7 mg, 0.295×10^{-3} mol) in THF/methanol (5 mL, 4:1 v/v), 28% sodium methoxide (0.12 mL, 0.589×10^{-3} mol) in methanol was added at room temperature. The reaction mixture was stirred at reflux temperature for 15 h. The mixture was neutralized with Dowex H^+. The product was washed with 20% methanol/dichloromethane, collected by filtration, and concentrated to dryness to give crude 3,6-di-*O*-benzyl cellulose (**8**). The crude compound **8** was ethylated without purification.

3,6-Di-*O*-benzyl-2-*O*-ethyl Cellulose (9)

To a solution of 3,6-di-*O*-benzyl cellulose (**8**) in DMSO (3 mL), 60% sodium hydride in mineral oil (61.4 mg, 1.50×10^{-3} mol, 5 equiv.) and ethyl iodide (118 μL, 1.50×10^{-3} mol, 5 equiv.) were added at room temperature. The reaction mixture was stirred at room temperature for 1 d. To the mixture, additional 60% sodium hydride in mineral oil (61.4 mg, 1.50×10^{-3} mol, 5 equiv.) and ethyl iodide (118 μL, 1.50×10^{-3} mol, 5 equiv.) were added. The reaction mixture was stirred at 50 °C for 2 d. A small amount of methanol was added in order to inactivate residual reagents. The reaction mixture was precipitated into distilled water. The precipitate was collected by filtration, and washed by distilled water and ethanol to give 3,6-di-*O*-benzyl-2-*O*-ethyl cellulose (**9**) (98.2 mg, 0.265×10^{-3} mol, 90% yield from compound **7**).

3,6-Di-*O*-acetyl-2-*O*-ethyl Cellulose (10)

To a solution of 3,6-di-*O*-benzyl-2-*O*-ethyl cellulose (**9**) (80.5 mg, 0.217×10^{-3} mol) in THF/acetic acid (1/1, v/v) (4 mL), 20% palladium hydroxide on carbon (150 mg) was added. The reaction mixture was kept under 400 kPa at 80 °C for 4 h. The reaction mixture was concentrated and treated with acetic anhydride (4 mL), pyridine (4 mL) and *N,N*-dimethylaminopyridine (40 mg) at 50 °C overnight. The product was washed with 20% methanol/dichloromethane and collected by filtration. The solution of crude compound was concentrated with ethanol to dryness. The crude compound was precipitated into distilled water. Purified compound was collected by filtration to give product (59.7 mg,

0.218×10^{-3} mol, 100%). After purification on a gel filtration column LH-20, 3,6-di-*O*-acetyl-2-*O*-ethyl cellulose (**10**) was obtained (33.6 mg, 0.113×10^{-3} mol, 56%).

2-*O*-Ethyl Cellulose (**1**)

To a solution of 3,6-di-*O*-acetyl-2-*O*-ethyl cellulose (**10**) (59.4 mg, 0.217×10^{-3} mol) in THF/methanol (10 mL, 4:1, v/v), 28% sodium methoxide (0.176 mL, 0.866×10^{-3} mol) in methanol was added at room temperature. The reaction mixture was stirred at reflux temperature for 17 h. The mixture was neutralized with Dowex H^+. The product was washed with 20% methanol/dichloromethane, collected by filtration, and concentrated to dryness to give crude 2-*O*-ethyl cellulose. The reaction mixture was concentrated to dryness. After dialysis against distilled water for 7d, the product was freeze-dried to give 2-*O*-ethyl cellulose (**1**) (29.2 mg, 70.7%).

^{1}H NMR (D_2O): $\delta = 1.19$ (CH_3CH_2O), 3.18 (H2), 3.2–4.1 (H3, H4, H5, H6, H6, OCH_2CH_3), 4.53 (d, $J = 7.5$, H1)

^{13}C NMR (D_2O): $\delta = 17.2$ (CH_3CH_2O), 62.5 (C6), 71.8 (CH_3 CH_2O), 76.3 (C3), 77.7 (C5), 80.8 (C4), 83.5 (C2), 104.9 (C1).

Synthesis Route for 3-*O*-Methyl Cellulose (**2**)

3-*O*-Ethyl-6-*O*-pivaloyl-α-D-glucopyranose 1,2,4-Orthopivalate (**5**)

To a solution of 3-*O*-ethyl-2,6-di-*O*-pivaloyl-D-glucopyranose (1.299 g, 3.45×10^{-3} mol) in CH_2Cl_2 (10 mL), triethylamine (1.44 mL, 10.35×10^{-3} mol) and benzenesulfonyl chloride (0.48 mL, 3.80×10^{-3} mol) was added at 0 °C. The reaction mixture was stirred at room temperature for 2.5 h. The mixture was concentrated and purified by silica gel column chromatography (eluent: methylenechloride/*n*-hexane = 1/2, v/v) to give a colorless oil (**5**) (846 mg, 68% yield).

^{1}H NMR ($CDCl_3$): $\delta = 1.05$ (s, 9H, $O_3C-C(CH_3)_3$), 1.23 (s, 9H, $OCOC(CH_3)_3$), 1.23 (t, 3H, J = 6.9, C3–OCH_2CH_3), 3.51–3.72 (m, 2H, C3–OCH_2CH_3), 3.86 (m, 1H, J = 4.5, 1.2, 1.4, H4), 4.19 (dd, 1H, J = 2.1, 4.8, H3), 4.28 (dd, 1H, J = 6.0, 11.1, H6), 4.38 (dd, 1H, J = 7.2, 11.4, H6), 4.45 (m, 1H, H2), 4.49 (broad t, J = 6.6, H5), 5.77 (d, 1H, J = 4.8, H1).

^{13}C NMR ($CDCl_3$): $\delta = 15.2$ (C3–OCH_2 CH_3), 24.7 ($O_3C-C(CH_3)_3$), 27.0 ($OCOC(CH_3)_3$), 35.6 (O_3 $C-C-(CH_3)_3$), 38.6 ($OCOC(CH_3)_3$), 64.3 (C6), 65.8 (C3–OCH_2CH_3), 71.3 (C3), 71.5 (C4), 72.1 (C2), 75.1 (C5), 97.4 (C1), 122.9 (O_3 C-C-$(CH_3)_3$), 178.1 ($OCOC(CH_3)_3$)

3-*O*-Ethyl-2,6-di-*O*-pivaloyl Cellulose (**11**)

Polymerization of 3-*O*-ethyl-6-*O*-pivaloyl-α-D-glucopyranose 1,2,4-orthopivalate (**5**) (193.7 mg, 0.54×10^{-3} mol) was carried out at −40 °C for 3 d and at room temperature for 5 min. 3-*O*-Ethyl-2,6-di-*O*-pivaloyl cellulose (140.4 mg, 72.5% yield) was obtained according to the general work-up procedure. No monomer remained after polymerization ($DP_n = 42.6$, $\overline{M}_n = 1.53 \times 10^4$, $\overline{M}_w/\overline{M}_n = 1.95$).

3-*O*-Ethyl Cellulose (**2**)

To a solution of 2,6-di-*O*-pivaloyl-3-*O*-ethyl cellulose (**11**) (108.5 mg, 0.303×10^{-3} mol) in THF/methanol (20 mL, 4:1, v/v), 28% sodium methoxide (0.25 mL, 1.212×10^{-3} mol) in methanol was added at room temperature. The reaction mixture was stirred at reflux temperature for 16 h. The mixture was neutralized with Dowex H^+. The product was washed with methanol, collected by filtration, and concentrated to dryness to give 3-*O*-ethyl cellulose (**2**) (53.9 mg, 94%).

^{1}H NMR (D_2O): $\delta = 1.18$ (CH_3CH_2O), 3.32 (H2), 3.4–3.6 (H3, H5), 3.65–3.9 (H4, H6, OCH_2CH_3), 3.9–4.1 (H6, OCH_2CH_3), 4.53 (d, $J = 7.5$, H1)

^{13}C NMR (D_2O): $\delta = 17.3$ (CH_3CH_2O), 62.8 (C6), 71.2 (CH_3 CH_2O), 76.0 (C2), 77.9 (C5), 78.7 (C4), 84.9 (C2), 104.8 (C1).

Synthesis Route for 6-*O*-Ethyl Cellulose (**3**)

3-*O*-Benzyl-6-*O*-ethyl-2-*O*-pivaloyl Cellulose (**12**)

Polymerization of 3-*O*-benzyl-6-*O*-ethyl-α-D-glucopyranose 1,2,4-orthopivalate (**6**) (140 mg, 0.384×10^{-3} mol) was carried out for 1 d at −10 °C. 3-*O*-Benzyl-6-*O*-ethyl-2-*O*-pivaloyl-cellulose (**12**) (117.3 mg, 83.8% yield) was obtained. No monomer remained after polymerization ($DP_n = 61.6$, $\overline{M}_n = 2.25 \times 10^4$, $\overline{M}_w/\overline{M}_n = 1.87$).

3-*O*-Acetyl-6-*O*-ethyl-2-*O*-pivaloyl Cellulose (**13**)

To a solution of 3-*O*-benzyl-6-*O*-ethyl-2-*O*-pivaloyl cellulose (**12**) (100.9 mg, 0.275×10^{-3} mol) in THF/acetic acid (1/1, v/v) (4 mL), 20% palladium hydroxide on carbon (150 mg) was added. The reaction mixture was kept under 400 kPa at 80 °C for 4.25 h. The reaction mixture was concentrated and treated with acetic anhydride (5 mL), pyridine (5 mL) and *N,N*-dimethylaminopyridine (50 mg) at 50 °C overnight. The product was washed with 20% methanol/dichloromethane and collected by filtration. The solution of crude compound was concentrated with ethanol to dryness. The crude compound was precipitated into distilled water. Purified compound was collected by filtration to give product (84.4 mg) with a small amount of benzyl groups. After a second debenzylation/acetylation procedure as same as the first one, 3-*O*-acetyl-6-*O*-ethyl-2-*O*-pivaloyl-cellulose (**13**) was obtained (103.3 mg).

6-*O*-Ethyl Cellulose (**3**)

To a solution of 3-*O*-acetyl-6-*O*-ethyl-2-*O*-pivaloyl cellulose (**13**) (80.1 mg, 0.333×10^{-3} mol) in THF/methanol (20 mL, 4:1, v/v), 28% sodium methoxide (0.21 mL, 1.01×10^{-3} mol) in methanol was added at room temperature. The reaction mixture was stirred at reflux temperature for 17 h. The mixture was neutralized with an aqueous solution of HCl. The reaction mixture was concentrated to dryness. After dialysis against distilled water for 3 d, the product was freeze-dried to give a crude 6-*O*-ethyl cellulose (121.7 mg). A part of the crude polymer (77.9 mg) was purified on Bio-Gel P-6 (fine) to give the purified 6-*O*-ethyl cellulose (**3**) (15.5 mg, 51% yield).

^{1}H NMR (D_2O): $\delta = 1.19$ (CH_3CH_2O), 3.34 (H2), 3.5–3.9 (H3, H4, H5, H6, H6, OCH_2CH_3), 4.43 (d, $J = 7.5$, H1).

^{13}C NMR (D_2O): $\delta = 16.8$ (CH_3CH_2O), 69.6 (CH_3 CH_2O), 70.7 (C6), 75.5 (C2), 76.1 (C5), 76.6 (C3), 80.9 (C4), 105.1 (C1).

Acknowledgements: This investigation was supported in part by a *Grant-in-Aid for Scientific Research from the Ministry of Education, Science, and Culture of Japan* (Nos. 18680009 and 21580205).

Received: October 27, 2009; Revised: December 21, 2009; Published online: March 9, 2010; DOI: 10.1002/mabi.200900392

Keywords: cellulose; gels; ring-opening polymerization; synthesis; thermal properties

[1] A. B. Savage, "Ethylcellulose", in: *Encyclopedia of Polymer Science and Technology*, H. F. Mark, N. G. Gaylord, N. M. Bikales, Eds. Interscience, New York 1965, p. 3/475.
[2] R. Donges, *Br. Polym. J.* **1990**, *23*, 315.
[3] I. Jullander, *Acta Chem. Scand.* **1955**, *9*, 1291.
[4] M. Karakawa, "Chemical Synthesis of High Regioselectively Methylated Celluloses by a Cationic Ring-Opening Polymerization", PhD Thesis, Graduate School of Agriculture, Kyoto University, Kyoto 2003.
[5] A. Koschella, T. Heinze, D. Klemm, *Macromol. Biosci.* **2001**, *1*, 49.
[6] H. Kamitakahara, A. Koschella, Y. Mikawa, F. Nakatsubo, T. Heinze, D. Klemm, *Macromol. Biosci.* **2008**, *8*, 690.
[7] H. Kamitakahara, T. Funakoshi, T. Takano, F. Nakatsubo, *Cellulose* **2009**, *16*, 1167.
[8] H. Kamitakahara, T. Funakoshi, S. Nakai, T. Takano, F. Nakatsubo, *Cellulose* **2009**, *16*, 1179.
[9] H. Kamitakahara, F. Nakatsubo, D. Klemm, *Cellulose* **2006**, *13*, 375.
[10] H. Kamitakahara, F. Nakatsubo, D. Klemm, *Cellulose* **2007**, *14*, 513.
[11] H. Kamitakahara, A. Yoshinaga, H. Aono, F. Nakatsubo, D. Klemm, W. Burchard, *Cellulose* **2008**, *15*, 797.
[12] H. Kamitakahara, F. Nakatsubo, *Cellulose* **2010**, *17*, 173.
[13] T. Kondo, *Carbohydr. Res.* **1993**, *238*, 231.
[14] A. Koschella, D. Fenn, T. Heinze, *Polym. Bull.* **2006**, *57*, 33.
[15] F. Nakatsubo, H. Kamitakahara, M. Hori, *J. Am. Chem. Soc.* **1996**, *118*, 1677.
[16] H. Kamitakahara, M. Hori, F. Nakatsubo, *Macromolecules* **1996**, *29*, 6126.
[17] A. Isogai, A. Ishizu, J. Nakano, *J. Appl. Polym. Sci.* **1984**, *29*, 3873.

Cellulose (2010) 17:923–936
DOI 10.1007/s10570-010-9437-3

Radially oriented cellulose triacetate chains on gold nanoparticles

Yukiko Enomoto-Rogers · Hiroshi Kamitakahara · Arata Yoshinaga · Toshiyuki Takano

Received: 29 March 2010 / Accepted: 13 July 2010 / Published online: 29 July 2010

Abstract Cellulose triacetate (CTA) derivatives having a disulfide group at the reducing-end (CTA2S, CTA13S, CTA41S), with number average degrees of polymerization (DP_ns) of 2, 13 and 41, respectively, were prepared. The CTA-self-assembled gold nanoparticles (CTA2Au, CTA13Au, and CTA41Au) were obtained through the reduction of gold salt ($HAuCl_4$) with CTASs. The diameters (d) and the interparticle distances (L) of the gold cores were analyzed by transmission electron microscopy (TEM) observations. The d values of CTA2Au, CTA13Au, and CTA41Au, were 8.7, 7.9, and 13.4 nm respectively. The L values of CTA2Au, CTA13Au, and CTA41Au, were 2.8, 6.3, and 20.9 nm, respectively, and agreed well with the molecular length (l) of CTAS chains (ls of CTA2S, CTA13S, CTA41S = 2.0, 7.5, 21.5 nm, respectively). The hydrodynamic diameters (D) of CTAAu nanoparticles in chloroform solution, measured by dynamic light scattering (DLS), were larger than the d values and increased with the increase in the molecular length of the CTA chains. The CTAS chain was found to work as an excellent stabilizer of the gold nanoparticles in both solid state and solution. The molecular length of CTA chains controlled the size and the alignment of the gold nanoparticles. As a result, the radially oriented CTA chains on the gold nanoparticles were successfully prepared.

Keywords Cellulose triacetate · Reducing-end · Gold nanoparticles · Orientation · Self-assembly

Introduction

Cellulose is a semi-rigid and linear (1 → 4)-β-glucopyranan. Cellulose molecule has a hemiacetalic hydroxyl group at the reducing-end, which has different reactivity from other hydroxyl groups and C2, C3, C6 positions (Arndt et al. 2003, 2005; Nakatsubo et al. 1987). Only a few approaches have been reported on the synthesis of cellulose-containing block copolymers, (Ceresa 1961; de Oliveira and Glasser 1994a, b; Feger and Cantow 1980; Kim et al. 1973, 1976; Mezger and Cantow 1983a, 1983b, 1984; Pohjola and Eklund 1977; Sipahi-Saglam et al. 2003; Stannett and Williams 1976; Steinmann 1970; Yagi et al. 2010). We have recently succeeded to prepare the novel well-defined cellulosic diblock copolymers by stepwise elongation of long-chain alkyl groups at the reducing-end of cellulose (Kamitakahara et al. 2005; Kamitakahara and Nakatsubo 2005). Based on our synthetic

Electronic supplementary material The online version of this article (doi:10.1007/s10570-010-9437-3) contains supplementary material, which is available to authorized users.

Y. Enomoto-Rogers · H. Kamitakahara (✉) · A. Yoshinaga · T. Takano
Division of Forest and Biomaterials Science, Graduate School of Agriculture, Kyoto University, Kitashirakawa-Oiwake-cho, Sakyo-ku, Kyoto 606-8502, Japan
e-mail: hkamitan@kais.kyoto-u.ac.jp

strategy, the self-assembling system of amphiphilic cellulosic diblock copolymers (Enomoto et al. 2006) and the structure of the branched copolymer with cellulosic side-chains (Enomoto-Rogers et al. 2009a, 2009b) have been investigated. However, it has been difficult to control supramolecular structure, such as orientation, of cellulose chains. Cellulose crystals with parallel orientation have not prepared from regenerated cellulose or *via* chemical synthetic pathway yet, although there have been some attempts to build up parallel orientation of the cellulose chains using cello-oligosaccharide analogues (Bernet et al. 2000; Murty et al. 2006).

Recently, in the field of engineering or biological applications, much attention have been paid to the colloidal gold nanoparticles due to their various functionalities, such as optical (Li et al. 2007a, 2007b; Link and El-Sayed 1999), electric (Maye et al. 2000), and catalytic (Haruta and Date 2001; Schubert et al. 2001) properties, depending on their size and size distribution (quantum size effect) or alignment (Daniel and Astruc 2004; Katz and Willner 2004). The stabilizer of the gold nanoparticles plays a crucial role in controlling size, size distributions, alignments, solubility, other physical or chemical properties, and functions of the obtained gold nanoparticles (Heath et al. 1997; Li et al. 2007a, 2007b; Yonezawa et al. 2001a, 2001b). It is well-known that sulfide compounds work as the stabilizer of gold nanoparticles *via* sulfide-gold bonding (Brust et al. 1994, 1995; Daniel and Astruc 2004; Katz and Willner 2004). Long-chain alkyl groups or polymers carrying thiol or disulfide groups have been widely studied for surface-modification of gold nanoparticles to develop new building blocks with various structure and properties (Brust et al. 1994, 1995; Corbierre et al. 2004; Li et al. 2007a, 2007b; Ohno et al. 2002; Yonezawa et al. 2001b).

Moreover, many studies on cellulose-gold nanocomposites have been reported as organic–inorganic hybrid material for engineering or biological applications, in last few years. Gold nanoparticles are mostly dispersed and immobilized on a surface or inside of cellulosic supporting material, such as films or membranes (Kumar et al. 2009; Liu et al. 2010; Loskutov et al. 2009), fibers (Li and Taubert 2009; Pinto et al. 2007; Yokota et al. 2008), nanocrystals (Shin et al. 2008), microcapsules (Lai et al. 2006).

Furthermore, cellulose triacetate is one of the most important cellulose derivatives and is an excellent material for functional films, membranes (Edgar et al. 2001; Glasser 2004; Sata et al. 2004). CTA chain exhibits good solubility in common organic solvents, but has lower flexibility, and stiff and extended structure in solutions compared to other flexible polymers such as polyisobutylene or poly(methyl methacrylate) (Fort et al. 1963; Howard and Parikh 1968). We anticipated that CTA having a sulfide group at the reducing-end might bind on gold nanoparticles and that it might form monolayer of CTA chains organized in a radial manner with head (the reducing-end)-to-tail (the non-reducing-end) orientation. In organic solutions such as chloroform, CTA having sulfide group is expected to work as a stabilizer of gold nanoparticles and to keep gold nanoparticles well-dispersed. In solid state such as a thin film, stiff CTA chain is expected to control interparticle distance of gold nanoparticles by the molecular length of CTA chains. Regarding self-assembled monolayers of cellulose derivatives which have recently been studied (Wenz et al. 2004, 2005), cellulose-self-assembled gold nanoparticles are expected to be a novel class of cellulosic material since cellulose chains are organized in a radial manner.

From a fundamental aspect, there have been some reports on crystalline polymorphs of cellulose and cellulose triacetate (CTA) (Kono et al. 1999, 2002). Both cellulose I and CTA I are accepted to have parallel orientation (Stipanovic and Sarko 1978; Sugiyama et al. 1991; Woodcock and Sarko 1980). On the other hand, both CTA II and cellulose II are believed to have anti-parallel orientation (Dulmage 1957; Kolpak and Blackwell 1976; Roche et al. 1986). It is known that CTA I is only obtained by heterogeneous acetylation of cellulose I while CTA II is obtained by homogeneous acetylation of cellulose I or acetylation of cellulose II (Sprague et al. 1958). It is also known that cellulose I and II are obtained by deprotection of CTA I and CTA II, respectively (Sprague et al. 1958). It is, therefore, of fundamental and technical interest to investigate structure of cellulose and CTA chains with a head-to-tail orientation.

Herein, we describe the preparation and characterization of cellulose derivatives carrying disulfide group at the reducing-end regioselectively and quantitatively, and describe the preparation and characterization of radially oriented CTA chains on the gold nanoparticles by means of TEM observations and DLS measurements.

Experimental

General Measurements

^{1}H-, ^{13}C-, and two-dimensional NMR spectra were recorded on a Varian INOVA300 FT-NMR (300 MHz) spectrometer, in $CDCl_3$ with tetramethylsilane (TMS) as an internal standard. Chemical shifts (δ) and coupling constants (J) are reported in (ppm) and (Hz), respectively. MALDI-TOF MS spectra were recorded on a Bruker REFLEX III with 2,5-dihydroxybenzoic acid (DHB) as a matrix in reflector or linear mode. Sephadex LH-20 was used for gel filtration chromatography.

GPC Measurement

Number and weight average molecular weights (M_n and M_w) and polydispersity index (M_w/M_n) were estimated by gel permeation chromatography (GPC) (CBM-10A, SPD-10A, SIL-10A, LC-10AT, FCV-10AL, CTO-10A, RID-10A, Shimadzu, Japan) in chloroform at 40°C. Shodex columns (K802, K802.5, and K805) were used. The flow rate was 1.0 ml/min. Calibration curves were obtained by using polystyrene standards (Shodex).

UV–vis measurements

UV–vis spectra were recorded on a JASCO V-560 spectrometer at 25°C. Chloroform solutions of the samples (0.1 mg/ml) were filtered with poly(tetrafluoroethylene) syringe filter (pore size of 0.2 μm) before the measurement.

TEM analysis

Transmission electron microscopy (TEM) images were collected by JEOL JEM-1220 system operating at an accelerating voltage of 100 kV. Samples were prepared by casting solution of CTA-self-assembled gold nanoparticles (CTAAu) in chloroform (0.1 mg/ml, 10 μl) on copper grids that were pre-coated by Formvar (polyvinyl formal) and reinforced by carbon. The samples were analyzed without staining with uranyl diacetate, because the CTA molecules could not be observed with the treatment of uranyl diacetate. The sizes of particles were calibrated using Latex Particles ϕ0.23 μm (Ohken Shoji, Japan). TEM images were recorded on Fuji FG films (Fuji Film, Japan). The image data of the films were printed on photographic papers at 6.3 magnifications. The developed images were stored with a general scanner at 300 dpi. TEM images were analyzed using public domain ImageJ program (Rasband, W.S., U.S. National Institutes of Health, Bethesda, Maryland, USA, http://rsb.info.nih.gov/ij/, 1997-2009). The diameter (d) and the interparticle distance (L) of the gold cores were obtained from measurements of at least 150 particles per sample. The diameter (d) was calculated from the area of the gold core on the assumption that the gold cores were circles. The interparticle distance (L) was defined as the distance from the edge of the each gold core to that of another adjacent particle.

DLS Measurements

Hydrodynamic diameters of gold nanoparticles were recorded on dynamic light scattering (DLS) spectrophotometer (ELS-Z2, Photal Otsuka Electronics) equipped with He–Ne laser (λ = 632.8 nm) at 25°C. Hydrodynamic diameters and intensity distribution histograms of the CTA-self-assembled gold nanoparticles were obtained by Cumulant method and Marquardt method, respectively (Gulari et al. 1979). Chloroform solutions of the samples (1.0 mg/ml) were filtered with poly(tetrafluoroethylene) syringe filter (pore size of 0.2 μm) before the measurement.

Materials

2,3,6-Tri-*O*-acetyl-4-*O*-(2,3,4,6-tetra-*O*-acetyl-β-D-glucopyranosyl)-β-D-glucopyranosylamine was prepared as described in our previous article (Kamitakahara and Nakatsubo 2005). Tri-*O*-acetyl-β-cellulosylamine (DP_n = 13) was prepared *via* five reaction steps as described in our previous article (Kamitakahara et al. 2005) from low-molecular-weight cellulose obtained from cellulose microcrystalline (CF-11, Whatman) using phospholic acid (Atalla et al. 1984; Isogai and Usuda 1991). Tri-*O*-acetyl-β-cellulosylamine (DP_n = 30) was obtained *via* six reaction steps from cellulose microcrystalline (Avicel, Merck) as described in our previous article (Kamitakahara et al. 2005). Tri-*O*-acetyl-β-cellulose (DP_n = 30) prepared at the third step was treated with acetic anhydride and pyridine at 60°C overnight at the fourth step for the complete acetylation of the residual hydroxyl group at the non-reducing-end,

which appeared after the depolymerization of CTA chain caused by HBr treatment at the second step, because these hydroxyl group were substituted by lipoyl group in the presence of DMAP, when they were not acetylated. DL-α-Lipoic acid (Tokyo Chemical Industry Co., Ltd., Japan) and hydrogen tetrachloroaurate (III) tetrahydrate ($HAuCl_4 \cdot 4H_2O$) (Wako Pure Chemical Industries, Ltd., Japan), sodium borohydride ($NaBH_4$) (Nakalai Tesque Co., Ltd., Japan), and all other reagents were commercially obtained and used without further purification.

N-lipoyl-2,3,6-tri-*O*-acetyl-4-*O*-(2,3,4,6-tetra-*O*-acetyl-β-D-glucopyranosyl)-β-D-glucopyranosylamine (CTA2S)

To a solution of DL-α-lipoic acid (330 mg, 2 eq), dicyclohexylcarbodiimide (DCC, 330 mg, 2 eq) and dimethylaminopyridine (DMAP, 130 mg, 2 eq) in dichloromethane (17.5 ml), 2,3,6-tri-*O*-acetyl-4-*O*-(2,3,4,6-tetra-*O*-acetyl-β-D-glucopyranosyl)-β-D-glucopyranosylamine (500 mg, 1 eq) was added, and stirred overnight at 0°C under nitrogen. After completion of the reaction, the mixture was filtered, washed with dichloromethane and the filtrate was concentrated to dryness. Crude product was purified by a silica gel column chromatography (eluent: ethyl acetate/*n*-hexane (2:1, v/v)) to give colorless solid (CTA2S) (0.57 g, 87.5% yield). ^{1}H-NMR ($CDCl_3$): δ 1.4 (2H, m, $C_1NHCOCH_2CH_2\mathit{CH_2CH_2}$), 1.6 (4H, m, $C_1NHCOCH_2\mathit{CH_2CH_2CH_2}$), 1.9 (1H, m, S–S-$CH_2C\mathit{H_2}$), 2.0–2.1 (21H, m, $\mathit{CH_3}CO$), 2.2 (2H, overlapped, $C_1NHCOC\mathit{H_2}$), 2.4 (1H, m, S–S-$CH_2C\mathit{H_2}$), 3.1 (2H, m, S–S-$C\mathit{H_2}$), 3.55 (1H, overlapped, S–S-$C\mathit{H}$), 3.61–3.70 (m, 1H, $C_{5'}$-H), 3.73–3.76 (m, 2H, C_4-H, C_5-H), 4.04 (dd, 1H, $J_{5',6'} = 2.4$, $J_{6'a,6'b} = 12.6$, $C_{6'}$-H_b), 4.13 (dd, 1H, $J_{5,6b} = 4.2$, $J_{6a,6b} = 12.0$, C_6-H_b), 4.37 (dd, 1H, $J_{5',6'} = 4.5$, $J_{6'a,6'b} = 12.3$, $C_{6'}$-H_a), 4.46 (d, 1H, $J_{6a,6b} = 12.6$, C_6-H_a), 4.50 (d, 1H, $J_{1',2'} = 7.8$ $C_{1'}$-H), 4.83 (t, 1H, $J_{2,3} = 9.6$, C_2-H), 4.93 (t, 1H, $J_{2',3'} = 8.6$, $C_{2'}$-H), 5.07 (t, 1H, $J_{4',5'} = 9.3$, $C_{4'}$-H), 5.14 (t, 1H, $J = 9.2$, $C_{3'}$-H), 5.20 (t, 1H, $J_{1,2} = 9.5$, C_1-H), 5.29 (br t, 1H, $J_{3,4} = 9.3$, C_3-H), 6.17 (d, 1H, $J_{NH,1} = 9.3$, $C_1N\mathit{H}$CO). ^{13}C-NMR ($CDCl_3$): δ 20.5, 20.6, 20.7 ($\mathit{CH_3}$CO), 24.7 ($C_1NHCOCH_2\mathit{CH_2}$), 28.7 ($C_1NHCOCH_2CH_2\mathit{CH_2}$), 34.5 ($C_1NHCOCH_2CH_2CH_2\mathit{CH_2}$), 36.2 ($C_1NHCO\mathit{CH_2}$), 38.4 (S–S-$\mathit{CH_2}$), 40.2 (S–S-$CH_2\mathit{CH_2}$), 56.3 (S–S-$\mathit{CH}$), 61.6 ($C_{6'}$), 61.8 ($C_6$), 67.7 ($C_{4'}$), 70.8 ($C_2$), 71.5 ($C_{2'}$), 71.9 ($C_{5'}$), 72.0 ($C_3$), 72.8 ($C_{3'}$), 74.4 ($C_5$), 76.2 ($C_4$), 78.0 ($C_1$), 100.6 ($C_{1'}$), 169.0, 169.3, 169.4, 170.3, 170.3, 170.5, 171.4 ($CH_3\mathit{CO}$), 172.9 ($C_1NH\mathit{CO}$). MALDI-TOF MS (positive reflector mode; DHB as matrix): $C_{34}H_{49}NO_{18}S_2$ Calcd. 823.24; Found $[M + Na]^+ = 846.31$, $[M + K]^+ = 862.29$. *Anal.* Calc. for $C_{34}H_{49}NO_{18}S_2$: C, 49.57; H, 5.99; N, 1.70; S, 7.78. Found: C, 49.14; H, 5.85; N, 1.79; S, 7.79.

N-lipoyl-tri-*O*-acetyl-β-cellulosylamine (CTA13S)

To a solution of DL-α-lipoic acid (103 mg, 10 eq), dicyclohexylcarbodiimide (DCC, 103 mg, 10 eq), and dimethylaminopyridine (DMAP, 61 mg, 10 eq) in dichloromethane (5 ml), tri-*O*-acetyl-β-cellulosylamine ($DP_n = 13$) (200 mg, 1 eq) was added, and stirred overnight at 0°C under nitrogen. The mixture was filtered, washed with dichloromethane and the filtrate and washings were concentrated to dryness. Crude product in dichloromethane was poured into methanol, filtered, and dried *in vacuo* to give an amorphous solid (CTA13S) (172 mg, 86.0% yield).

^{1}H-NMR ($CDCl_3$): δ 1.4 (2H, m, $C_1NHCOCH_2\ CH_2\mathit{CH_2CH_2}$), 1.6 (4H, m, $C_1NHCOCH_2\mathit{CH_2CH_2}\ \mathit{CH_2}$), 1.8 (1H, m, S–S-$CH_2C\mathit{H_2}$), 1.9–2.1 (9H, m, $\mathit{CH_3}CO$), 2.2 (2H, overlapped, $C_1NHCOC\mathit{H_2}$), 2.4 (1H, m, S–S-$CH_2C\mathit{H_2}$), 3.1 (2H, m, S–S-$C\mathit{H_2}$), 3.56 (C_5-H), 3.6 (1H, overlapped, S–S-$C\mathit{H}$)), 3.72 (t, $J_{4,5} = 9.3$, C_4-H), 4.08 (d, $J = 7.2$, C_6-H_b), 4.37–4.48 (C_6-H_a, C_1-H), 4.80 (t, $J_{2,3} = 8.6$, C_2-H), 5.07 (t, $J_{3,4} = 9.3$, C_3-H), 6.11 (d, $J_{NH,\ 1} = 9.3$, $C_1N\mathit{H}CO$). ^{13}C-NMR ($CDCl_3$): δ 20.4, 20.5, 20.7 ($\mathit{CH_3}CO$), 24.6 ($C_1NHCOCH_2\mathit{CH_2}$), 28.7 ($C_1NHCOCH_2CH_2\mathit{CH_2}$), 34.4 ($C_1NHCOCH_2CH_2CH_2\mathit{CH_2}$), 36.1 ($C_1NHCO\ \mathit{CH_2}$), 38.3 (S–S-$\mathit{CH_2}$), 40.1 (S–S-$CH_2\mathit{CH_2}$), 56.2 (S–S-$\mathit{CH}$), 61.9 ($C_6$), 71.6 ($C_2$), 72.4 ($C_5$), 72.6 ($C_3$), 74.4 ($C_4$ at the reducing-end), 75.9 (C_4), 77.8 (C_1 at the reducing-end), 100.4 (C_1), 169.2, 169.6, 170.1 ($CH_3\mathit{CO}$ of C_2, C_3, C_6, respectively). MALDI-TOF MS (positive linear mode; DHB as matrix): DP = 7: $C_{94}H_{129}NO_{58}S_2$ Calcd. 2263.66; Found $[M + Na]^+ = 2289.55$, $[M + K]^+ = 2304.84$. DP = 8: $C_{106}H_{145}NO_{66}S_2$ Calcd. 2551.75; Found $[M + Na]^+ = 2578.05$, $[M + K]^+ = 2594.03$. DP = 9: $C_{118}H_{161}NO_{74}S_2$ Calcd. 2839.83; Found $[M + Na]^+$

= 2865.88, $[M + K]^+$ = 2882.02. DP = 10: $C_{130}H_{177}NO_{82}S_2$ Calcd. 3127.92; Found $[M + Na]^+$ = 3153.91, $[M + K]^+$ = 3169.91. DP = 11: $C_{142}H_{193}NO_{90}S_2$ Calcd. 3416.00; Found $[M + Na]^+$ = 3441.52, $[M + K]^+$ = 3457.55. DP = 12: $C_{154}H_{209}NO_{98}S_2$ Calcd. 3704.08; Found $[M + Na]^+$ = 3729.43, $[M + K]^+$ = 3745.35. DP = 13: $C_{166}H_{225}NO_{106}S_2$ Calcd. 3992.17; Found $[M + Na]^+$ = 4016.90, $[M + K]^+$ = 4032.41. DP = 14: $C_{178}H_{241}NO_{114}S_2$ Calcd. 4280.25; Found $[M + Na]^+$ = 4304.37, $[M + K]^+$ = 4320.37. DP = 15: $C_{190}H_{257}NO_{122}S_2$ Calcd. 4568.34; Found $[M + Na]^+$ = 4591.53, $[M + K]^+$ = 4607.20. DP = 16: $C_{202}H_{273}NO_{130}S_2$ Calcd. 4856.42; Found $[M + Na]^+$ = 4879.05, $[M + K]^+$ = 4894.84. DP = 17: $C_{214}H_{289}NO_{138}S_2$ Calcd. 5144.51; Found $[M + Na]^+$ = 5166.39, $[M + K]^+$ = 5182.18. DP = 18: $C_{226}H_{305}NO_{146}S_2$ Calcd. 5432.59; Found $[M + Na]^+$ = 5453.70, $[M + K]^+$ = 5468.45. DP = 19: $C_{238}H_{321}NO_{154}S_2$ Calcd. 5720.68; Found $[M + Na]^+$ = 5740.79, $[M + K]^+$ = 5756.04.

N-lipoyl-tri-*O*-acetyl-β-cellulosylamine (CTA41S)

The same procedure was applied to tri-*O*-acetyl-β-cellulosylamine (DP_n = 30) to obtain CTA41S (DP_n = 41). The increase in DP_n of CTA41S is due to the loss of low molecular fraction caused by the precipitation procedure.

Preparation of CTA 2Au

To a solution of *N*-lipoyl-2,3,6-tri-*O*-acetyl-4-*O*-(2,3,4,6-tetra-*O*-acetyl-β-D-glucopyranosyl)-β-D-glucopyranosylamine (2 mg) in 1,4-dioxane/H_2O (9:1, 20 ml), $HAuCl_4 \cdot 4H_2O$ (95 mg, 100 eq. of CTA2S) was added. After 3 min, a freshly prepared 0.1 M aqueous $NaBH_4$ solution (2 eq. of $HAuCl_4 \cdot 4H_2O$) was added dropwise with vigorous stirring. The solution turned dark reddish purple immediately. After further stirring for 4 h at room temperature, the solution was evaporated and extracted with chloroform, washed with water, and concentrated to dryness. Crude products were purified by gel filtration column chromatography (LH-20) with methanol/chloroform (1:4, v/v) to remove the residual CTA2S, concentrated, to give dark purple solid CTA2Au (12.7 mg).

Preparation of CTA13Au and CTA41Au

To a solution of *N*-lipoyl-tri-*O*-acetyl-β-cellulosylamine (CTA13S: 10 mg and CTA41S: 20 mg) in 1,4-dioxane/H_2O (9:1, 200 ml), $HAuCl_4 \cdot 4H_2O$ (103 mg and 69 mg, 100 eq. to CTA13S and CTA41S, respectively) was added. After 3 min, a freshly prepared 0.1 M aqueous $NaBH_4$ solution (2 eq. of $HAuCl_4 \cdot 4H_2O$) was added dropwise with vigorous stirring. The solution turned dark reddish purple immediately. After further stirring for 4 h at room temperature, the solution was evaporated and extracted with chloroform, washed with water, and concentrated to dryness. The crude product was sonicated briefly with ca.30% chloroform/methanol at least three times to remove the residual CTAS, dissolved in chloroform, filtered with poly(tetrafluoroethylene) syringe filter (pore size of 0.2 μm) to remove remaining aggregates of gold, and concentrated to dryness, to give dark purple solid CTA13Au (44.0 mg) and CTA41Au (56.6 mg).

Results and Discussion

Synthesis of CTASs

Lipoic acid is widely used as a sulfide linker, because it has both a disulfide group and a carboxyl group at each end of the molecule. Cellobiose and cellulose derivatives, *N*-lipoyl-2,3,6-tri-*O*-acetyl-4-*O*-(2,3,4,6-tetra-*O*-acetyl-β-D-glucopyranosyl)-β-D-glucopyranosylamine (CTA2S) and *N*-lipoyl-tri-*O*-acetyl-β-cellulosylamine (CTA13S and CTA41S) (DP_n = 13 and 41, respectively), were prepared from 2,3,6-tri-*O*-acetyl-4-*O*-(2,3,4,6-tetra-*O*-acetyl-β-D-glucopyranosyl)-β-D-glucopyranosylamine and tri-*O*-acetyl-β-cellulosylamine, using DCC and DMAP, as described in Fig. 1. The number and weight average molecular weights (M_n and M_w) and the polydispersity index (M_w/M_n), the number average degrees of polymerization (DP_ns) of the CTASs are summarized in Table 1. The M_ns of CTA13S and CTA41S were 4.11×10^3 and 12.1×10^3, respectively. The MALDI-TOF MS spectra of the CTASs are shown in Fig. 2. The observed molecular weights with each DP value agreed well with their calculated molecular weights, indicating quantitative substitution of the reducing-end by lipoyl group. The chemical structures of the CTASs were identified by ^1H-, ^{13}C, and

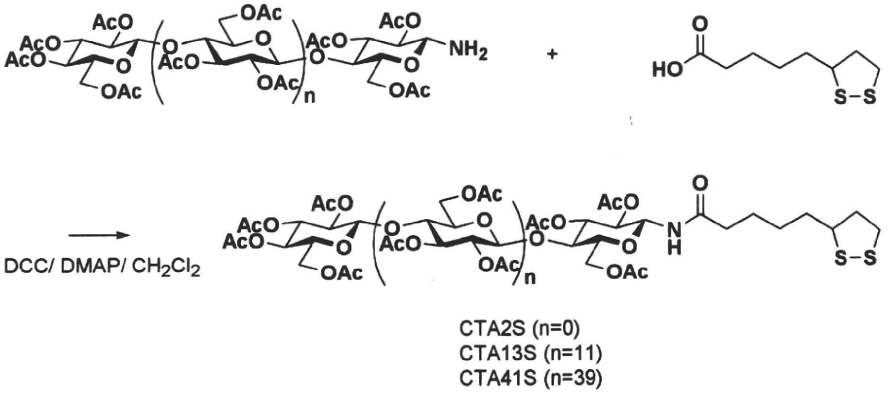

Fig. 1 Preparation of *N*-lipoyl-tri-*O*-acetyl-*β*-cellulosylamine

Table 1. Characteristics of CTASs

Samples	M_n (10^{-3})[a]	M_w (10^{-3})[a]	M_w/M_n[a]	DP_n[c]
CTA2S		0.8[b]		2
CTA13S	4.1	5.4	1.30	13.4
CTA41S	12.1	21.7	1.79	41.1

[a] Estimated by polystyrene standards with chloroform as eluent

[b] Theoretical molecular weight of CTA2S is 823.88

[c] Number average degree of polymerization of CTA chain

two-dimensional NMR measurements. The representative H–H gCOSY spectrum of CTA13S is shown in Fig. 3. The peaks assigned to lipoyl group and amide protons (C1-N*H*, δ 6.11 ppm) are observed. The correlation between the ring-proton (C1-H at the reducing-end, δ 5.19 ppm) and the amide proton (C1-N*H*, δ 6.11 ppm) indicates the formation of the amide linkage. The same correlation was observed in the H–H gCOSY spectrum of CTA41S.

Preparation of CTA-self-assembled gold nanoparticles

CTA2S, CTA13S, and CTA41S and $HAuCl_4 \cdot 4H_2O$ in 1,4-dioxane/water were treated with $NaBH_4$ (Brust et al. 1994). The colors of the solutions turned reddish purple, indicating the formation of gold nanoparticles. The gold nanoparticles obtained from CTA2S, CTA13S, and CTA41S are described as CTA2Au, CTA13Au, and CTA41Au, respectively. The UV–vis spectra and the images of chloroform solutions of the obtained gold nanoparticles are shown in Fig. 4. The absorption band at λ = ca. 530 nm in UV–vis spectra are assigned to the surface plasmon band of gold

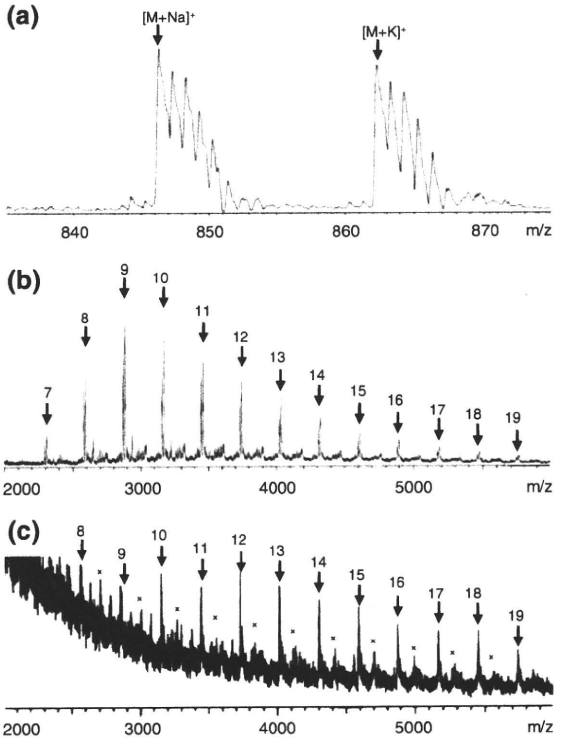

Fig. 2 MALDI-TOF MS spectra of **a** CTA2S, **b** CTA13S and **c** CTA41S. The numbers refer to the degree of polymerization

nanoparticles with the size of about 5-20 nm (Brust and Kiely 2002), indicating the formation of CTA-self-assembled gold nanoparticles. When the CTA (DP_n = 13) and $HAuCl_4 \cdot 4H_2O$ were treated with $NaBH_4$ as a control experiment, the solution turned black and the bulk gold aggregates precipitated immediately. As a result, the solution showed no surface plasmon band (Fig. 4d) because CTA chains without disulfide groups were not bound to the gold surface.

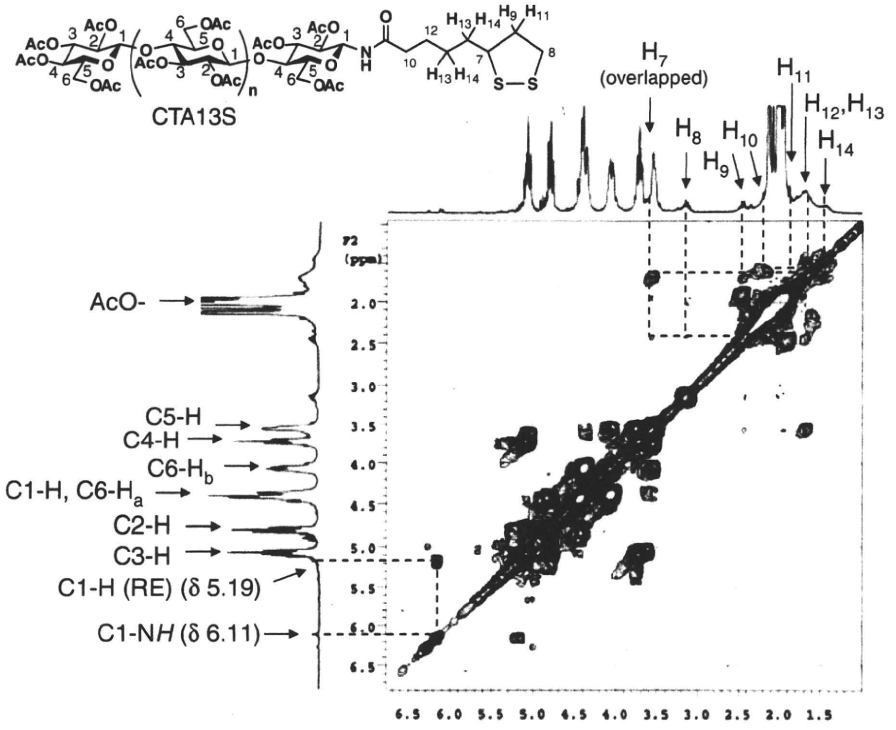

Fig. 3 H-H gCOSY spectrum of CTA13S

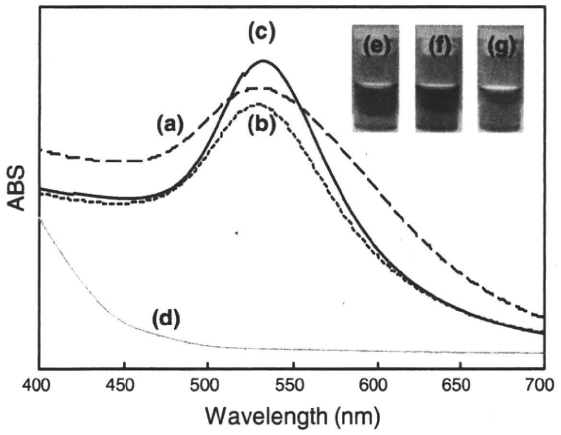

Fig. 4 UV-vis spectra and images of chloroform solutions (0.1 mg/ml) of **a**, **e** CTA2Au, **b**, **f** CTA13Au, **c**, **g** CTA41Au and **d** gold treated with $NaBH_4$ and CTA (DP_n = 13)

Furthermore, the concentration of initial $HAuCl_4 \cdot 4H_2O$ was investigated with the range from ca. 0.5 mg/ml to ca. 50 mg/ml, to optimize the condition for preparation of stable and uniformly dispersed CTAAu nanoparticles. When CTA2Au were prepared at higher initial $HAuCl_4 \cdot 4H_2O$ concentration (50 mg/ml), the bulk gold aggregates were formed and precipitated immediately. When the CTAAu particles were prepared at lower initial $HAuCl_4 \cdot 4H_2O$ concentration (0.5 mg/ml), the obtained particles were unstable, turned insoluble, and precipitated irreversibly in organic solvent such as chloroform after the purification. Consequently, the initial $HAuCl_4 \cdot 4H_2O$ concentration for CTA2Au was determined to be 5.0 mg/ml. When the CTA13Au and the CTA41Au were prepared at the higher initial $HAuCl_4 \cdot 4H_2O$ concentration (5.0 or 3.5 mg/ml), the bulk gold aggregates were formed and precipitated in some cases. The initial $HAuCl_4 \cdot 4H_2O$ concentrations for CTA13Au and CTA41Au were determined to be 0.5 and 0.35 mg/ml, respectively. These results revealed that the size and the size distribution of the gold nanoparticles increased with the increase in the initial $HAuCl_4 \cdot 4H_2O$ concentration.

The amount of $HAuCl_4 \cdot 4H_2O$ were also examined at 1, 10, 100, and 1,000 equivalents to CTASs. The maximum amount of $HAuCl_4 \cdot 4H_2O$ capable of being dispersed with CTAS chains was 100 equivalents to CTASs. At higher amount of $HAuCl_4 \cdot 4H_2O$ (1000 eq. to CTAS), most part of the gold were obtained as

bulk aggregates, and yield of CTAAu particles were very low. The previous researchers have studied the gold nanoparticles dispersed with the polymeric stabilizer (Azzam and Eisenberg 2007; Corbierre et al. 2004; Wuelfing et al. 1998), but the reported initial ratios of the gold to the polymer (Au/polymer) were 1 to 12, and relatively lower than those in our present study. Regarding previous results that Au/polymer compositions in the obtained gold nanoparticles were higher than initial Au/polymer composition (Corbierre et al. 2004; Wuelfing et al. 1998), we consider that large amount of polymer chains without sulfur atom were removed as a by-product by purification from the gold nanoparticles, and that only small amount of polymer with sulfur group were bound on the gold in those previous studies. On the other hand, there is an example that gold nanoparticles were only covered in polymer micelles, which are formed by hydrophobic interactions and are not chemically bound to the gold (Azzam and Eisenberg 2007). In our study, the CTAS chains have disulfide group at the reducing-end quantitatively, and they had the ability to stabilize significantly large amount of gold nanoparticles (100 eq. to CTAS).

The CTA2Au particles were purified by gel filtration chromatography to remove the unbound CTA2S, but only trace of CTA2S was removed. The CTA13Au or CTA41Au nanoparticles were first purified by dialysis against 1,4-dioxane with Wako dialysis membrane (12–14 k MWCO, regenerated cellulose), but free CTA13S or CTA41S were not detected outside of the membrane, confirmed by MALDI-TOF MS. Further purification was performed by sonication with ca. 30% chloroform/methanol, which dissolves CTAS selectively under this chloroform content. Complete purification was carried out by repeated washing with ca. 30% chloroform/methanol at least three times until the MS peaks of free CTA13S or CTA41S in CTAAu mixture became negligible. Further sonication disrupted the gold colloid obviously, because the reddish purple solution turned clear and the black precipitate was formed. The obtained CTA2Au, CTA13Au, and CTA41Au particles could be stored in solid state for more than a couple of month without degradation and still dissolved in organic solvents such as chloroform. CTA2Au, CTA13Au and CTA41Au were kept well-dispersed in chloroform at least for several days, indicating effective protection of gold nanoparticles

Table 2 Characteristics of CTAAu nanoparticles

Samples	Diameter of Au core (d) (nm) [a]			Interparticle distance of Au cores (L) (nm)[a]			Theoretical length of CTAS chains (l) (nm)[b]	CTAS in CTAAu (wt%/mol%)[c]	Surface Area of Au core (S) (nm^2) (10^{-2})[d]	Number of CTAS chains on Au core (10^{-2})[d]	Density of CTAS chains (ρ_{CTAS}) (chains/nm^2)[d]	Occupied Area per CTAS chain ($Å^2$)[d]	Interchain distance of CTAS chains (Å)[d]	Calculated diameter of CTAAu ($D_{calc.}$) (nm)[e]	Hydrodynamic diameter of CTAAu (D) (nm)[f]
	AVE	SD	CV	AVE	SD	CV									
CTA2Au	8.7	1.4	0.2	2.8	0.7	0.3	2.0	15.7/4.1	2.4	9.1	3.8	26.1	5.1	12.7	16.6
CTA13Au	7.9	3.2	0.4	6.3	1.6	0.3	7.5	22.7/1.4	2.0	2.2	1.1	90.9	9.5	22.9	49.0
CTA41Au	13.4	6.3	0.5	20.9	5.2	0.2	21.5	35.1/0.9	5.6	6.6	1.2	86.0	9.3	56.4	69.5

[a] Determined by TEM analysis. AVE: average, SD: standard deviation, CV: coefficient of variance. CV = SD/AVE

[b] Theoretical values of CTAS chain in streched conformation. The length of lipoyl chain in all-*trans* conformation = 1.0 nm

[c] Determined from initial feed of CTA and of Au and yield of CTAAu initial molar ratio [CTAS]/[Au] = 1/100

[d] Radius, surface area, and volume of Au core : $r = d/2$, $S = 4\pi r^2$ and $V = 4/3(\pi r^3)$, respectively. Density: ρ(Au) = 19.32 g/cm^3, Atomic mass: M(Au) = 196.96, Avogadro's constant: $N_A = 6.03 \times 10^{23}$, Occupied area per CTAS chain = (Interchain distance of CTAS chains)^2. Molecular weight: M(CTA2S) = 823.88, M_n(CTA13S) = 4.1×10^3 (estimated with PS standards), M_n(CTA41S) = 12.1×10^3 (estimated with PS standards)

[e] $D_{calc.} = d + 2\,l$

[f] Determined by DLS measurements

by CTAS layer. Only CTA2Au precipitated in chloroform after several days suggesting relatively effective protection of the gold by CTAS polymeric chains. It was found that the CTASs worked as excellent stabilizer of the gold nanoparticles both in the solution and in the solid such as a film.

TEM observations

The CTAAu particles were analyzed by transmission electron microscopy (TEM). The CTAS molecules were not negatively stained with the treatment of uranyl diacetate, indicating that the particles in TEM images were only gold cores. The characteristics of CTAAu visible nanoparticles are summarized in Table 2. According to the average diameters (d) of the gold cores, theoretical molecular length (l), and calculated diameter ($D_{calc.} = d+2\ l$) of CTAAu nanoparticles, the ideal and average images of single particles of CTA2Au, CTA13Au, and CTA41Au were illustrated in Fig. 5 on the assumption that gold cores were sphere, and that all CTA chains had the degree of polymerization of DP_n estimated by polystyrene standards.

The TEM images of gold nanoparticles of CTA2Au, CTA13Au, and CTA41Au, are shown in Fig. 6a, e, i, respectively. The size distribution histograms of the diameters (d) are shown in Fig 6c, g, k. The ds of the gold cores of CTA2Au, CTA13Au, and CTA41Au were 8.7, 7.9, and 13.4 nm, respectively. The d of CTA41Au with longer CTAS chain length was larger than those of CTA2Au and CTA13Au. It has been reported that the diameter of the gold nanoparticles tend to increase when they protected by the stabilizer with higher molecular weight or more steric hindrance (Corbierre et al. 2004; Yonezawa et al. 2001b). The interparticle distance (L) was defined as the distance from the edge of the each gold core to that of another adjacent particle, as described in Fig. 6b, f, j. The size distribution histograms of the interparticle distance (L) of the gold cores are shown in Fig 6d, h, l. The Ls of the gold cores of CTA2Au, CTA13Au, and CTA41Au, were 2.8, 6.3, and 20.9 nm, respectively, and agreed well with the theoretical molecular length of CTAS chains, where the ls of CTA2S, CTA13S, and CTA41S = 2.0, 7.5, and 21.5 nm, respectively. It has also been reported that the interparticle distances of the gold nanoparticles increased with

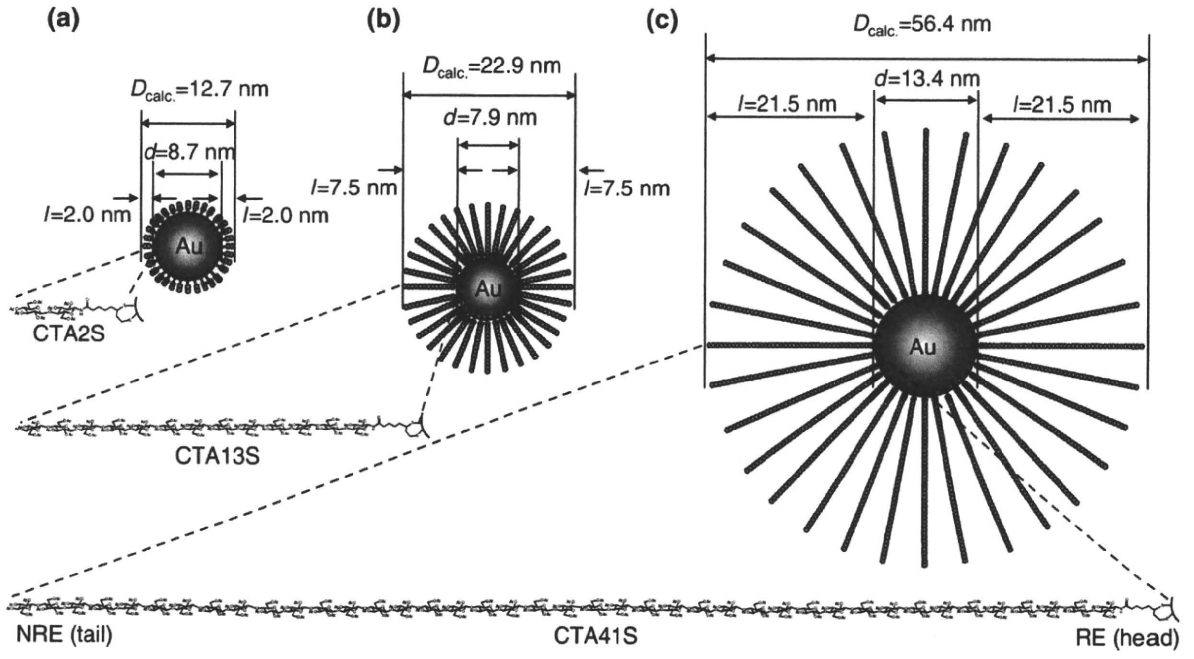

Fig. 5 Average images of a single particle of **a** CTA2Au, **b** CTA13Au, and **c** CTA41Au

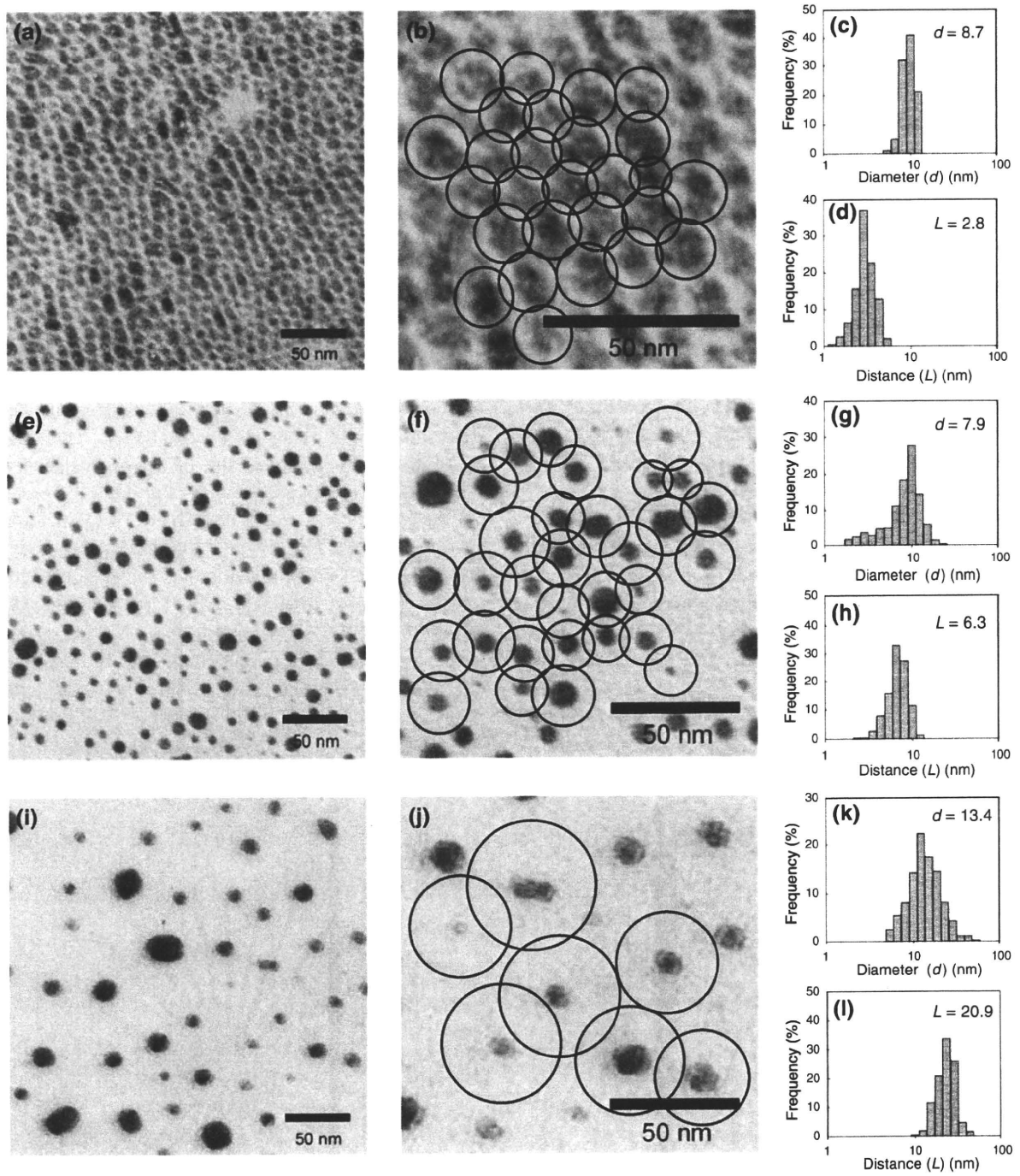

Fig. 6 **a**, **e**, **i** TEM images, **b**, **f**, **j** the assumed circles around the gold cores to measure the interparticle distances (L), the size distributions of **c**, **g**, **k** the diameters (d) and **d**, **h**, **l** the interparticle distances (L) of the gold cores. **a**, **b**, **c**, **d** CTA2Au, **e**, **f**, **g**, **h** CTA13Au, and (**i**, **j**, **k**, **l** CTA41Au, respectively

the increase in the molecular weight of protecting polymers (Corbierre et al. 2004; Ohno et al. 2002). In our experiments, the stiff CTA chains were expected to act as spacers between the gold cores, and they overlapped as described in Fig. 7a. It was suggested that the CTAS chains bound in a radial manner on the

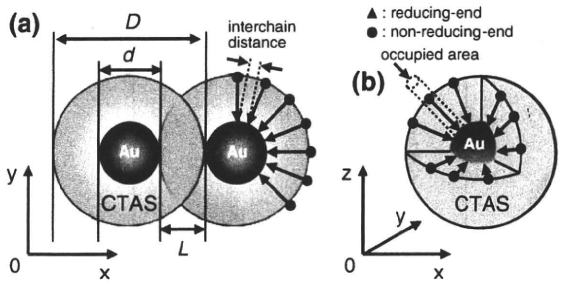

Fig. 7 Schematic drawings of CTAAu nanoparticles

gold cores in a head-to-tail orientation, where the reducing-end and the non-reducing-end are a head and a tail, respectively, as described in Fig. 7b. Thus, the interparticle distance of the gold nanoparticles were successfully controlled with the length of CTA chain.

Moreover, the surface areas of the gold cores, the numbers of CTAS chains on the gold, the densities (ρ_{CTAS}) of CTAS chains per nm^2, the occupied area per CTAS chain, the interchain distance of CTAS chains were calculated from the weight composition of CTAS and Au and the d values. The density (ρ_{CTAS}) of CTA2S chains was 3.8/nm^2. The occupied area per CTA2S chain and the interchain distance values were calculated to be 26.1 Å^2 and 5.1 Å, respectively, which are similar to those of alkanethiol-protected gold nanoparticles (Corbierre et al. 2004; Strong and Whitesides 1988; Yonezawa et al. 2001a, 2001b), for example, 21.4 Å^2 and 4.97 Å in the case of docosyl mercaptan (Strong and Whitesides 1988). Cellobiose acetate (CTA2) moiety had smaller steric hindrance and stabilized the gold nanoparticles as good as alkanethiol. Interestingly, the ρ_{CTAS} values of CTA13S and CTA41S chains were calculated to be nearly the same value, 1.1 and 1.2/nm^2 and occupied area per CTAS chain was 90.4 and 85.9 Å^2, respectively. The structure of CTAS is similar to that of poly(styrene) (PS) or poly(ethylene oxide) (PEO) because they are polymeric chains. Therefore, the occupied areas of CTAAus were compared with those of the gold nanoparticles which were protected efficiently by other common flexible polymers (Corbierre et al. 2004). The occupied areas of CTAAus were similar to those of the gold nanoparticles protected with PS ($DP_n = 125$) (83 Å^2) or PEO chains ($DP_n = 45$) (83 Å^2) prepared in the previous study, suggesting efficient protection of the gold with CTAS.

It is reported that the diameter of the gold nanoparticles stabilized with the "conical" di-chain-alkanethiol, 4,4′-dithiobis-(*N*-propyl-*O*,*O*′-ditetradecanoyl-L-glutamate ($d = 2.0$ nm, $l = 3.0$ nm) (Yonezawa et al. 2001a) with less steric hindrance were smaller than that protected with mono-chain-dodecanthiol ($d = 2.7$ nm $l = 1.8$ nm,) (Strong and Whitesides 1988). However, the occupied area of the "conical" di-chain-alkanethiol and of the mono-chain-alkanethiol were similar to each other (23.3 Å^2 (Yonezawa et al. 2001b) and 21.4 Å^2 (Strong and Whitesides 1988), respectively). It was suggested that the CTA41S chains with longer chain-length had larger steric hindrance, and that the diameter (d) of the gold cores increased compared to those of CTA2Au and CTA13Au. The standard deviations of the L of CTA13Au and CTA41Au tended to be larger than that of CTA2Au, due to the polydispersity of the CTAS chains.

DLS measurements

The hydrodynamic diameters (D) of the CTAAu nanoparticles in chloroform solution were determined by DLS measurements, and listed in Table 2. The intensity distribution histograms of the CTAAu were shown in Fig. 8. In DLS measurement, the larger particles exhibit much stronger intensity even when their number is very small. CTA13Au nanoparticles have larger standard deviation (SD) value of size distribution of the gold cores and polydispersity of CTA chains. We consider that the bimodal distribution of intensity is just a result of analysis of scattering data calculated by Marquardt method. These D values indicated that the gold nanoparticles were well-dispersed in nano-scale in chloroform and that the CTAS chains worked as an excellent stabilizer in the solution. The hydrodynamic diameter indicates the total diameter of nanoparticles with the gold core and the CTA shell (Corbierre et al. 2004; Li et al. 2007a, 2007b). The average diameters (D) of CTA2Au, CTA13Au, and CTA41Au were all larger than the average diameter (d) of the gold core as shown in Figs. 6c, g, k, 8a, b, c, respectively. The Ds were larger than calculated diameter ($D_{calc.} = d + 2\,l$) values of the CTAAu. It is known that the diameter of the micelles swollen or moving in the solution is calculated larger than that of the micelles shrinking in the solid state (Azzam and Eisenberg

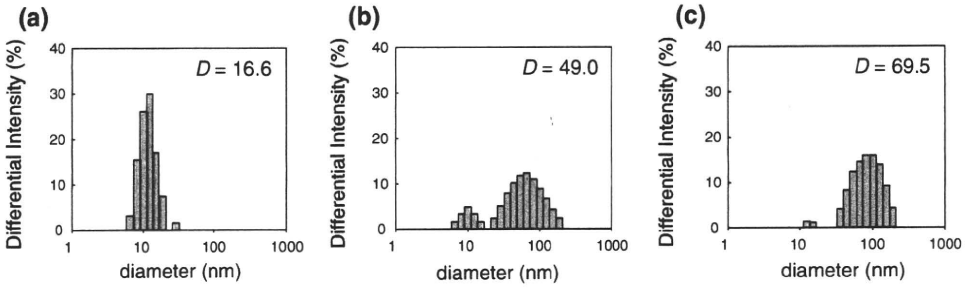

Fig. 8 Intensity distribution histograms of **a** CTA2Au, **b** CTA13Au, and **c** CTA41Au in chloroform (1.0 mg/ml). Hydrodynamic diameters were obtained by Cumulant method. Intensity distribution histograms were obtained by Marquardt method

2007). In our case, the interparticle distance (L) values of the gold cores in the thin film observed in TEM images were smaller than the interparticle distance values in solution, which were expected to be larger than $2l$, as shown in Figs. 5 and 7. This fact supports the interdigitation of CTA chains of CTAAu in the film observed in TEM images, as described in Fig. 7a. In addition, the D values showed no difference after 1 day, indicating the stability of CTAAu nanoparticles in the solution. These facts strongly indicated that the CTAS chains bound covalently on the gold nanoparticles with the core–shell structure, and that the length of CTA chains controlled the thickness of the CTA shell.

Conclusions

CTA-self-assembled gold nanoparticles (CTAAu) were prepared *via* reduction of gold salt with the cellulose triacetate derivatives having a disulfide group at the reducing-end (CTA2S, CTA13S, and CTA41S). A method to control the size and alignment of gold nanoparticles by the molecular weight of CTA was successfully demonstrated. CTAAu nanoparticles had a well-defined core–shell structure with gold as a core and CTA as a shell radially oriented around the gold core in head-to-tail orientation. Interparticle distances of the gold nanoparticles in the film of CTAAu agreed well with the length of stiff CTA chains. The nanocomposite of CTA and gold can be applied for novel organic–inorganic hybrid cellulosic materials, such as an additive for cellulosic polymer blends to control the density of gold nanoparticles, or self-assembled monolayers (SAM) of cellulosic chains on a planar gold surface for engineering applications in the future.

Acknowledgments This study was supported in part by a Grand-in-Aid from a Research Fellowships of the Japan Society for the Promotion of Science (JSPS) for Young Scientists (Y.E-R), and by a Grant-in-Aid for Scientific Research from the Ministry of Education, Science, and Culture of Japan (Nos. 18688009 and 21580205).

References

Arndt P, Bockholt K, Gerdes R, Huschens S, Pyplo J, Redlich H, Samm K (2003) Cellulose oligomers: preparation from cellulose triacetate, chemical transformations and reactions. Cellulose 10:75–83

Arndt P, Gerdes R, Huschens S, Pyplo-Schnieders J, Redlich H (2005) Preparation of cellulose oligomers from cellulose triacetate (standard procedure). Cellulose 12:317–326

Atalla RH, Ellia JD, Schroeder LR (1984) Some eeffects of elevated temperatures on the structure of cellulose and its transformation. J Wood Chem Technol 4:465–482

Azzam T, Eisenberg A (2007) Monolayer-protected gold nanoparticles by the self-assembly of micellar poly (ethylene oxide)-b-poly(epsilon-caprolactone) block copolymer. Langmuir 23:2126–2132

Bernet B, Xu JW, Vasella A (2000) Oligosaccharide analogues of polysaccharides part 20—NMR analysis of templated cellodextrins possessing two parallel chains: A mimic for cellulose I. Helv Chim Acta 83:2072–2114

Brust M, Kiely CJ (2002) Some recent advances in nanostructure preparation from gold and silver particles: A short topical review. Colloids Surf A-Physicochem Eng Aspects 202:175–186

Brust, M., Walker, M., Bethell, D., Schiffrin, D.J. and Whyman, R. (1994) Synthesis of thiol-derivatized gold nanoparticles in a 2-phase liquid-liquid system. Journal of the Chemical Society-Chemical Communications 801–802

Brust, M., Fink, J., Bethell, D., Schiffrin, D.J. and Kiely, C. (1995) Synthesis and reactions of functionalized gold nanoparticles. Journal of the Chemical Society-Chemical Communications 1655–1656

Ceresa RJ (1961) The synthesis of block and graft copolymers of cellulose and its derivatives. Polymer 2:213–219

Corbierre MK, Cameron NS, Lennox RB (2004) Polymer-stabilized gold nanoparticles with high grafting densities. Langmuir 20:2867–2873

Daniel MC, Astruc D (2004) Gold nanoparticles: Assembly, supramolecular chemistry, quantum-size-related properties, and applications toward biology, catalysis, and nanotechnology. Chem Rev 104:293–346

de Oliveira W, Glasser WG (1994a) Multiphase materials with lignin. 13. Block-copolymers with cellulose propionate. Polymer 35:1977–1985

de Oliveira W, Glasser WG (1994b) Novel cellulose derivatives. 2. Synthesis and characteristics of mono-functional cellulose propionate segments. Cellulose 1:77–86

Dulmage WJ (1957) The molecular and crystal structure of cellulose triacetate. J Polym Sci 26:277–288

Edgar KJ, Buchanan CM, Debenham JS, Rundquist PA, Seiler BD, Shelton MC, Tindall D (2001) Advances in cellulose ester performance and application. Prog Polym Sci 26: 1605–1688

Enomoto Y, Kamitakahara H, Takano T, Nakatsubo F (2006) Synthesis of diblock copolymers with cellulose derivatives. 3. Cellulose derivatives carrying a single pyrene group at the reducing-end and fluorescent studies of their self-assembly systems in aqueous NaoH solutions. Cellulose 13:437–448

Enomoto-Rogers Y, Kamitakahara H, Nakayama K, Takano T, Nakatsubo F (2009a) Synthesis and thermal properties of poly(methyl methacrylate)-graft-(cellobiosylamine-C15). Cellulose 16:519–530

Enomoto-Rogers Y, Kamitakahara H, Takano T, Nakatsubo F (2009b) Cellulosic graft copolymer: Poly(methyl methacrylate) with cellulose side chains. Biomacromolecules 10:2110–2117

Feger C, Cantow HJ (1980) Cellulose containing block co-polymers. 1. Synthesis of trimethylcellulose-(b-poly (oxytetramethylene))-star block co-polymers. Polym Bull 3:407–413

Fort RJ, Hutchinson RJ, Moore WR, Murphy M (1963) Viscosity temperature relationships for dilute solutions of high polymers. Polymer 4:35–46

Glasser WG (2004) Prospects for future applications of cellulose acetate. Macromol Symp 208:371–394

Gulari E, Gulari E, Tsunashima Y, Chu B (1979) Photon-correlation spectroscopy of particle distributions. J Chem Phys 70:3965–3972

Haruta M, Date M (2001) Advances in the catalysis of au nanoparticles. Appl Catal A-Gen 222:427–437

Heath JR, Knobler CM, Leff DV (1997) Pressure/temperature phase diagrams and superlattices of organically functionalized metal nanocrystal monolayers: the influence of particle size, size distribution, and surface passivant. J Phys Chem B 101:189–197

Howard P, Parikh RS (1968) Solution properties of cellulose triacetate. 2. Solubility and viscosity studies. J Polym Sci A Polym Chem 6:537–546

Isogai A, Usuda M (1991) Preparation of low-molecular-weight celluloses using phosphoric-acid. Mokuzai Gakkaishi 37:339–344

Kamitakahara H, Nakatsubo F (2005) Synthesis of diblock copolymers with cellulose derivatives. 1. Model study with azidoalkyl carboxylic acid and cellobiosylamine derivative. Cellulose 12:209–219

Kamitakahara H, Enomoto Y, Hasegawa C, Nakatsubo F (2005) Synthesis of diblock copolymers with cellulose derivatives. 2. Characterization and thermal properties of cellulose triacetate-block-oligoamide-15. Cellulose 12:527–541

Katz E, Willner I (2004) Integrated nanoparticle-biomolecule hybrid systems: synthesis, properties, and applications. Angew Chem-Int Ed 43:6042–6108

Kim S, Stannett VT, Gilbert RD (1973) New class of biodegradable polymers. J Polym Sci C-Polym Lett 11:731–735

Kim S, Stannett VT, Gilbert RD (1976) Biodegradable cellulose block copolymers. J Macromol Sci-Chem A 10: 671–679

Kolpak FJ, Blackwell J (1976) Determination of structure of cellulose II. Macromolecules 9:273–278

Kono H, Numata Y, Nagai N, Erata T, Takai M (1999) Studies of the series of cellooligosaccharide peracetates as a model for cellulose triacetate by ^{13}C CP/MAS NMR spectroscopy and x-ray analyses. Carbohydr Res 322: 256–263

Kono H, Erata T, Takai M (2002) CP/MAS ^{13}C NMR study of cellulose and cellulose derivatives. 2. Complete assignment of the ^{13}C resonance for the ring carbons of cellulose triacetate polymorphs. J Am Chem Soc 124:7512–7518

Kumar R, Pandey AK, Tyagi AK, Dey GK, Ramagiri SV, Bellare JR, Goswami A (2009) In situ formation of stable gold nanoparticles in polymer inclusion membranes. J Colloid Interf Sci 337:523–530

Lai MK, Chang CY, Lien YW, Tsiang RCC (2006) Application of gold nanoparticles to microencapsulation of thioridazine. J Control Release 111:352–361

Li ZH, Taubert A (2009) Cellulose/gold nanocrystal hybrids via an ionic liquid/aqueous precipitation route. Molecules 14:4682–4688

Li DX, Cui Y, Wang KW, He Q, Yan XH, Li JB (2007a) Thermosensitive nanostructures comprising gold nanoparticles grafted with block copolymers. Adv Funct Mater 17:3134–3140

Li DX, He Q, Cui Y, Wang KW, Zhang XM, Li JB (2007b) Thermosensitive copolymer networks modify gold nanoparticles for nanocomposite entrapment. Chem-A Eur J 13:2224–2229

Link S, El-Sayed MA (1999) Size and temperature dependence of the plasmon absorption of colloidal gold nanoparticles. J Phys Chem B 103:4212–4217

Liu Z.M, Li M, Turyanska L, Makarovsky O, Patane A, Wu WJ, Mann S (2010) Self-assembly of electrically conducting biopolymer thin films by cellulose regeneration in gold nanoparticle aqueous dispersions. Chemistry of Materials 22:2675–2680

Loskutov AI, Uryupina OY, Vysotskii VV, Roldughin VI (2009) Surface faceting of gold nanoparticles and adsorption of organic macromolecules. Colloid J 71: 668–671

Maye MM, Lou YB, Zhong CJ (2000) Core-shell gold nanoparticle assembly as novel electrocatalyst of co oxidation. Langmuir 16:7520–7523

Mezger T, Cantow HJ (1983a) Cellulose containing block copolymers. 4. Cellulose triester macroinitiators. Angew Makromol Chem 116:13–27

Mezger T, Cantow HJ (1983b) Cellulose containing block copolymers. 5. Threeblock co-polymer syntheses via macroinitiator. Makromol Chem-Rapid Commun 4:313–320